Gondwana Research, V. 5, No. 4, pp. 781-800.

ISSN: 1342-937X

GR Gondwana Research

A Vendian-Cambrian Island Arc System of the Siberian Continent in Gorny Altai (Russia, Central Asia)

M.M. Buslov[1], T. Watanabe[2]*, I.Yu. Saphonova [1], K. Iwata[2], A. Travin[1] and M. Akiyama[3]

[1] *United Institute of Geology, Geophysics and Mineralogy, Russian Academy of Sciences, Siberian Branch, 630090, Koptyuga ave. 3, Novosibirsk, Russia, E-mail: inna@uiggm.nsc.ru*

[2] *Division of Earth and Planetary Sciences, Graduate School of Science, Hokkaido University, 060-0810, Sapporo, Japan*

[3] *Consulting Engineers I.N.A.Corporation, Bunkyo-ku, 112-8668, Tokyo, Japan*

(Manuscript received December 5, 2001; accepted May 23, 2002)

Abstract

An extended Vendian-Cambrian island-arc system similar to the Izu-Bonin-Mariana type is described in the Gorny Altai terrane at the margin of the Siberian continent.

Three different tectonic stages in the terrane are recognized. (1) A set of ensimatic active margins including subducted oceanic crust of the Paleo-Asian ocean, the Uimen-Lebed primitive island arc, oceanic islands and seamounts: the set of rocks is assumed to be formed in the Vendian. (2) A more evolved island arc comprising calc-alkaline volcanics and granites: a fore-arc trough in Middle-late Cambrian time was filled with disrupted products of pre-Middle Cambrian accretionary wedges and island arcs. (3) Collision of the more evolved island arc with the Siberian continent: folding, metamorphism and intrusion of granites occurred in late Cambrian-early Ordovician time.

In the late Paleozoic, the above-mentioned Caledonian accretion-collision structure of the Siberian continent was broken by large-scale strike-slip faults into several segments. This resulted in the formation of a typical mosaic-block structure.

Key words: Paleo-Asian ocean, island arc, eclogite, Gorny Altai, Central Russia.

Introduction

The available reconstructions of the Paleo-Asian ocean or the equivalent ocean (Zonenshain et al., 1990; Sengor et al., 1993; Didenko et al., 1994; Didenko, 1997; Scotese and McKerrow, 1990; McKerrow et al., 1992) assumed that, in Vendian time, it existed in between Siberia and East Gondwana and could be up to 4000 km wide. The western and southern margins of the Siberian continent were bounded by an island arc system – Kuznetsk-Altai-Khantaishirin. Remnants of island arcs have been found in South Siberia and Mongolia (Fig. 1) and their ages are believed to be Vendian-Cambrian by many investigators of the Altai Mountains. Gorny Altai is a western mountainous part of the Altai-Sayan area (ASA), which is a Caledonian accretion-collisional complex of South Siberia containing large fragments of Vendian-Cambrian island arcs formed after the closing of the Paleo-Asian ocean (Zonenshain et al., 1990; Berzin and Dobretsov, 1994; Dobretsov et al., 1995; Buslov et al., 1993, 2001). The most comprehensive and advanced examination for the Vendian-Cambrian island arcs in the Altai-Sayan region is discussed by Buslov et al. (2001).

Buslov et al. (2001) proposed a newly defined terrane classification and revealed that the Gorny Altai terrane preserved a set of island arc systems in Vendian-Cambrian time near the Paleo-Asian ocean/Siberian continent border. In the present-day structural pattern of the Gorny Altai terrane the fragments of Vendian-early Cambrian ophiolites, island arcs and paleo-oceanic islands are separated by late Paleozoic faults. Buslov et al. (2001) also proposed late Carboniferous-early Permian reactivated suture zones along the Kazakhstan and Siberian continents (Fig. 2).

This paper presents more advanced results of the study of structure, age, composition and fossils of island arc units in the southeastern part (Kurai zone) of the Gorny Altai terrane at the southern and central parts of the Kurai Range. In spite of loose chronological constraints as described later, Ar–Ar dates and fossil data indicate that

* *Deceased*

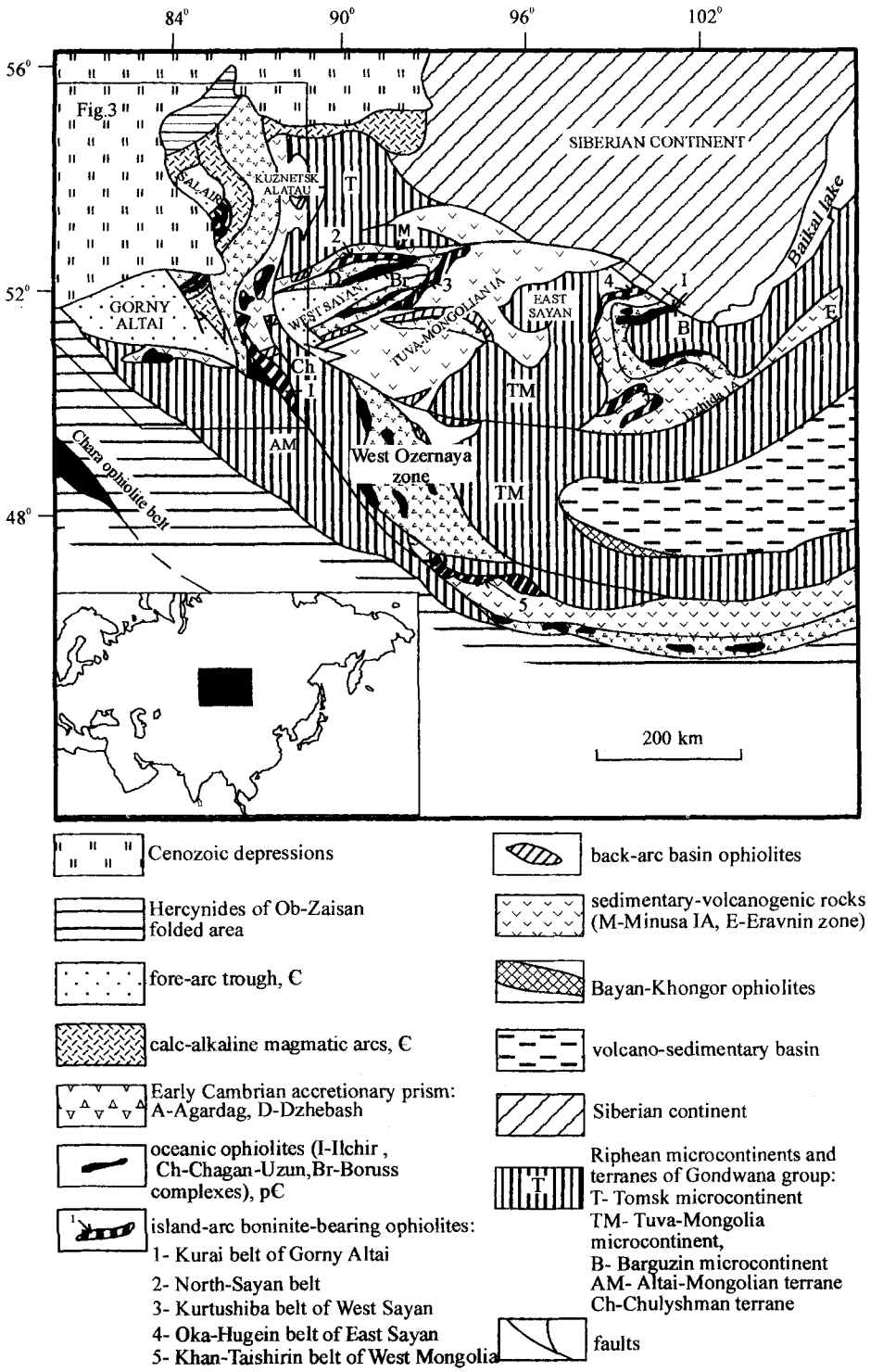

Fig. 1. Distribution of Caledonian accretion-collision zones and Precambrian microcontinents of the Gondwana and Eurasia groups in the Altai-Sayan region on the southern side of the Siberian continent (Dobretsov et al., 1995). IA = Island Arc system (Tuva-Mongolian IA, Dzhida IA, Munisa IA).

Vendian-Cambrian rocks are predominant in the Gorny Altai terrane.

Outline of Geology in the Kurai Zone

The Kurai zone consists of well-preserved fragments of the island arc system. They compose the following three units bounded by faults mainly from the west to the east, i.e., (1) Middle-late Cambrian rocks (Anui-Chuya fore-arc trough), (2) Kurai accretionary wedge and (3) Uimen-Lebed island arc (Figs. 3, 4). They compose a nappe-sheeted structure (Figs. 4, 5). The Kurai zone is bounded by strike-slip faults dipping to the northeast on the northern margin. The northern side is occupied by the

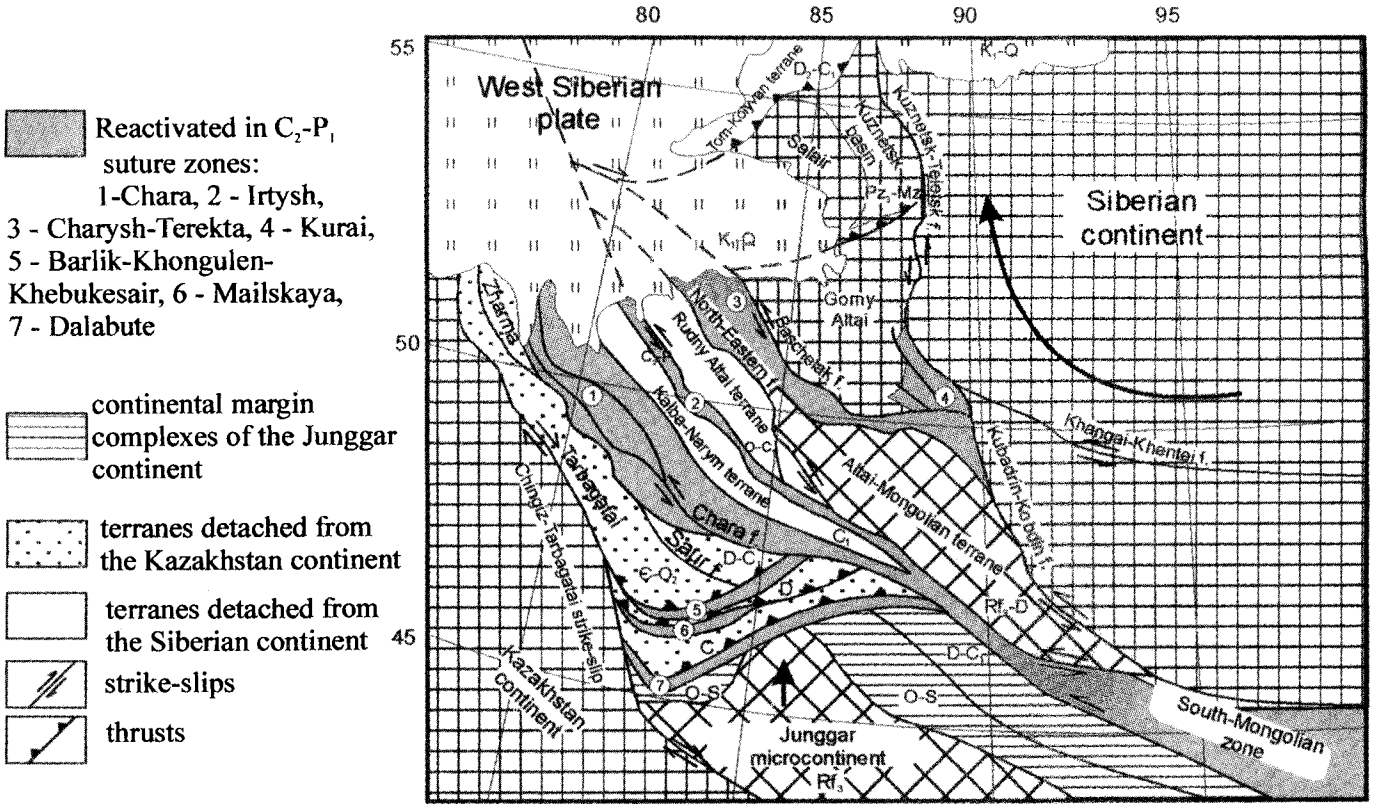

Fig. 2. Suture zones along the Siberian and Kazakhstan continents reactivated in late Carboniferous–early Permian time (Buslov et al., 2001).

Altai-Mongolian terrane and the Teletsk terrane which might be a fragmented Gondwana supercontinent (Buslov et al., 2001). Since the palaeontological data have been obtained only from rocks in the Anui-Chuya fore-arc trough, we shall describe these rocks first.

Geology of Rock Units

Anui-Chuya fore-arc basin (Middle-Upper Cambrian)

In the Anui-Chuya basin, various kinds of boulders derived from island arcs and accretionary wedges including mid-oceanic ridge basalt (MORB) have been found. The boulders were probably supplied from the eastern units (accretionary wedge and arc) and the tectonic setting, therefore, is fore-arc. The fore-arc basin complex near Aktash Village (Figs. 6, 7), referred to as the Chibit Formation hereinafter, has the following structure and composition (Buslov et al., 1998). Olistostromes and conglomerates occur among rhythmically alternating sand- and siltstones, compositionally and structurally proximal to the Gorny Altai flysch in the inner Anui-Chuya basin. The sandstones are green and gray, chiefly polymictic or, less often, quartz-feldspathic; the clays are gray and lilac, clay or clay-carbonaceous, with scattered green, purple, or red siliceous-argillaceous and siliceous interbeds. The bedding is generally rhythmical, starting with sands and finishing with siltstones, mudstones, or sometimes, siliceous facies. Coarse-grained facies exist as lenses and interbeds of olistostromes, conglomerates, or sandy gritstones, up to hundreds of meters thick. All the terrigenous deposits, together with basal conglomerate horizons, overlie the accretionary complex (Buslov, 1992; Buslov et al., 1993). Towards the basin axis (the western side), coarse-grained facies are less important and, as a rule, are reduced to random conglomerate lenses and isolated pebble beds. The Anui-Chuya terrigenous clastics are degraded fragments of different structures (metamorphic terrane, accretionary complex, primitive island arc) similar to the rocks of Uimen-Lebed arc origin and a more evolved island arc partially preserved in the Kurai Zone. The olistostrome and the Gorny Altai flysch complexes show intricate relations with local lateral transitions and concordant or discordant vertical interbedding. Thus, paleontological studies of the olistostrome complex can help dating the Gorny Altai Group in the Anui-Chuya Zone. The upper limit of the Group is marked by its unconformable boundary with the overlaying paleontologically constrained Arenig (Lower Ordovician) Voskresenka Formation in northwestern Gorny Altai (Petrunina et al., 1984).

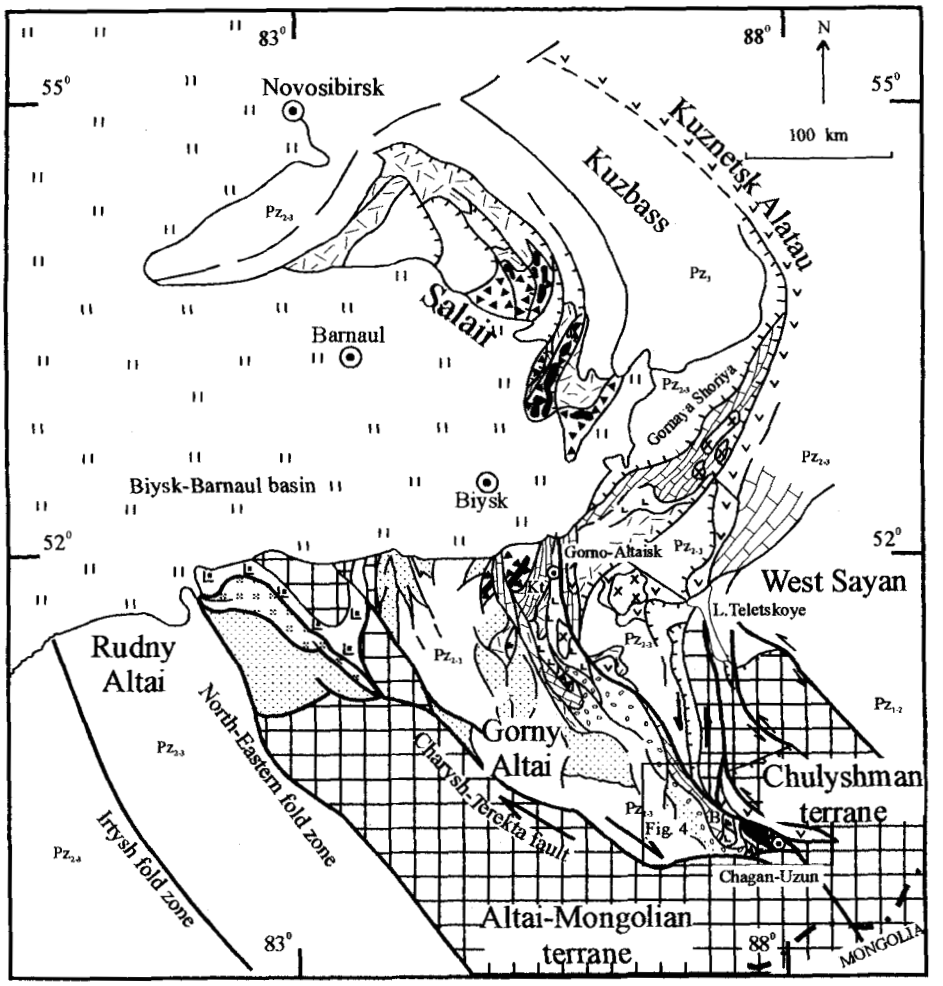

Fig. 3. Geological sketch map of the Vendian–early Cambrian island arc in Gorny, Salair and Kuznetsk Alatau (Buslov et al., 2001).

We add below new results of paleontological and stratigraphic studies of the olistostrome and silt-sandstone formations in the Chibit-Aktash-Baratal area in the middle course of the Chuya River.

The terrigenous rocks of the Gorny Altai Group in the southeastern margin of the Anui-Chuya basin overlie the carbonaceous Baratal Formation with unconformity (Buslov, 1992; Bondarenko, 1976; Buslov et al., 1993) (Fig. 6). The thickness of the basal coarse-clastic horizon, which was examined north of Aktash village, changes abruptly in the southwestern direction from 2 to 200 m within a distance of 1 km. The basal horizon has an extremely complicated structure. In its thickest part it is represented by boulder-size conglomerates and breccias that give way westward to a few irregularly striking interbeds and lenses of breccias, conglomerates and

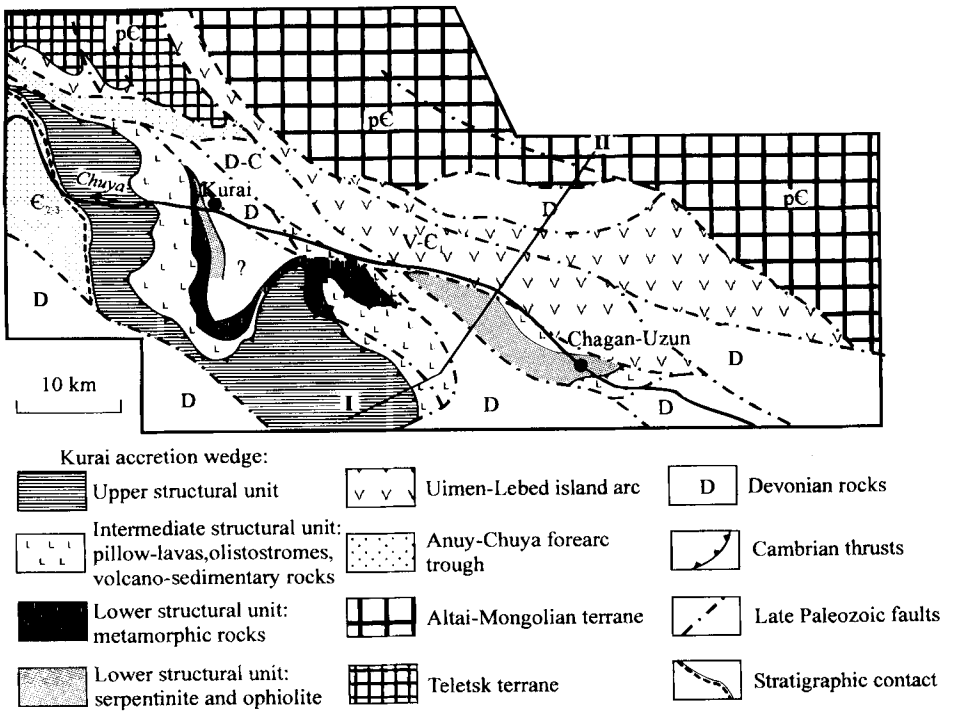

Fig. 4. Simplified geological-structural scheme of the Kurai zone.

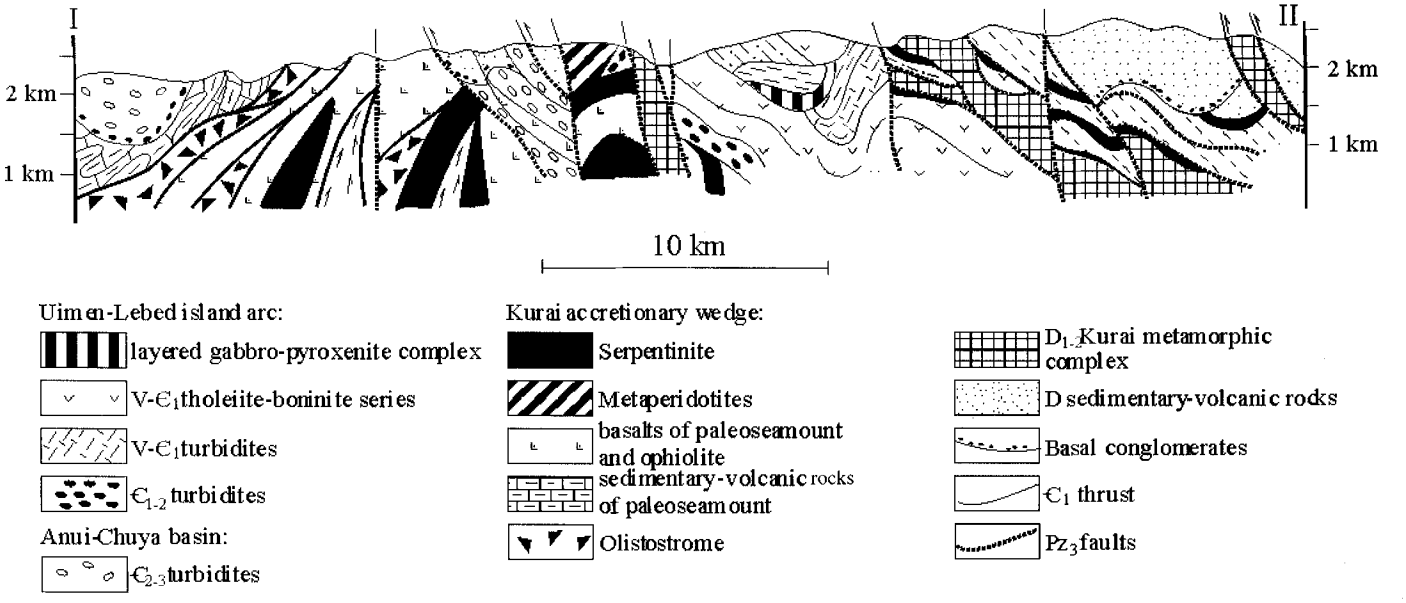

Fig. 5. The section across the Kurai zone.

gritstones in a matrix of alternating polymictic sandstones and siltstones. The coarse-grained facies lie upon the uneven surface of the Baratal limestones. Immediately below the surface, siliceous rocks rise among carbonates as ~1 m high peaks formed by selective paleoweathering. Rock fragments in the boulder conglomerates are, as a rule, poorly rounded gray and black marbleized limestones and dolomites with siliceous concretions and interlayers, or black, green and red jaspers. The basal horizon locally includes small sand- and siltstone lenses, 2–3 cm thick and up to 10 cm long, that can be syndepositional xenoclasts. The boulder conglomerates and breccias are overlain by alternated sandstones and shales with rare coarse-grained lenses up to 1 m thick and 5 m long.

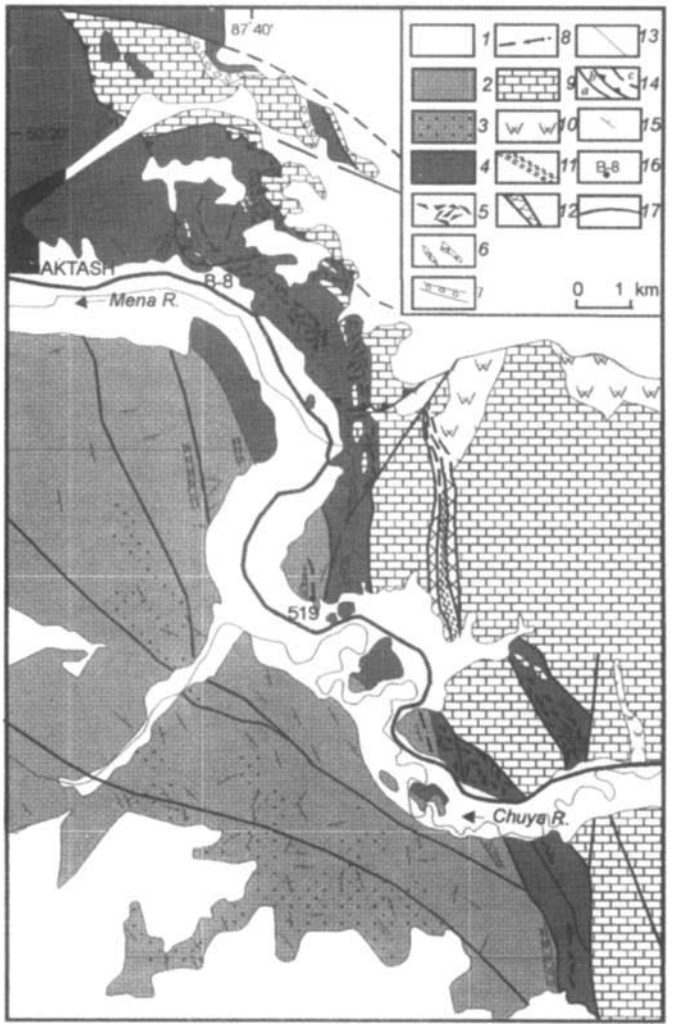

Fig. 6. Geological sketch map of the Anui-Chuya fore-arc basin. 1–recent deposits; 2-8–Middle-late Cambrian basin slope facies: 2, 3–variegated formation: 2–rhythmically alternating sandstones, siltstones and shales, 3–prevalently sandstone members; 4–Chibit Formation; 5–olistostromes; 6–olistoplaques of siliceous-carbonate deposits; 7–polymictic conglomerates; 8–interbeds of variegated jaspers; 9, 10–rocks of the late Vendian–early Cambrian accretionary complex: 9–siliceous-carbonate deposits of the Baratal Formation, 10–silicilites; 11–early Cambrian siltstones and sandstones of littoral facies of oceanic islands; 12–subductional melange; 13–stratigraphic boundaries; 14–faults: a–strike-slip faults, b–oblique thrusts, c–hypothetic faults; 15–bedding direction; 16–sites for fossil sampling; 17–Chuya motor-road.

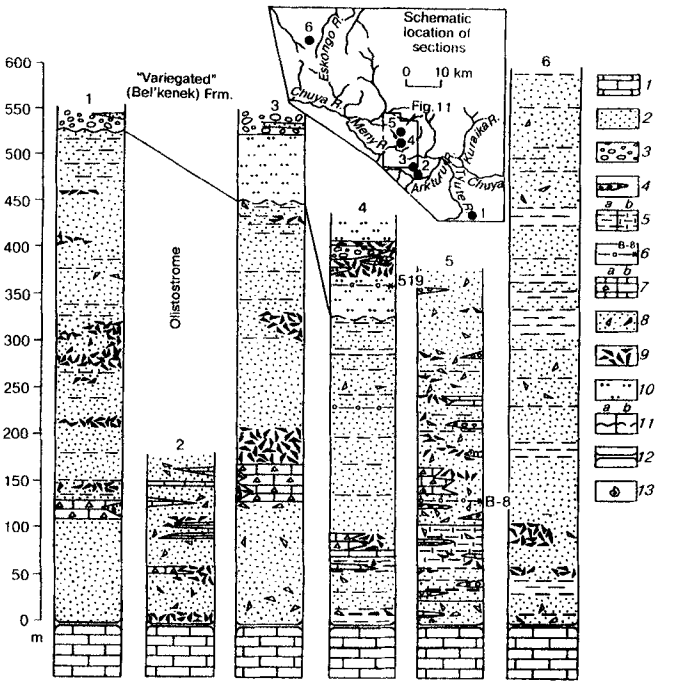

Fig. 7. Columnar sections of the Anui-Chuya basin along the Menka River.

In the source of the Menka River, the terrigenous complex and the Baratal Formation have a non-coherent contact. Near it, the Baratal limestones are cut with fractures as deep as a few meters, filled in with limestone clastics or polymictic sandstones. Above the contact, sandstones contain poorly rounded fragments of limestones and siliceous rocks of different sizes and shapes, the basal horizon attaining a thickness of few tens of meters. Further upward there is a 50 m thick layer of interbedded sandstones and siltstones with <50 cm thin and 3–5 m long lenses of coarse-grained facies; it is followed by the olistostrome complex traceable for over 8 km along its boundary with the Baratal Formation.

Examined in the upper course of the Menka River (right side), the complex consists of the following strata (described upsection) (see columnar sections in Fig. 7):

1. Gray carbonate-clayey and argillaceous siltstones involving randomly scattered elongated lenses of Baratal olistoliths and smaller clasts of limestones and silicilites oriented along the member bedding. The apparent thickness of the largest exposed olistolith attains 8 m, its length exceeding 25 m.

2. A horizon of Baratal limestone olistoplaques attaining a length of 750 m.

3. Gray and dark-green, poorly sorted polymictic sandstones, gritstones and conglomerates with sporadic inclusions of several centimeters long clasts of marbleized limestones, dolomites, and silicilites of variable roundness. The sandstones locally contain purple and red siliceous interbeds, from which sponge spicules were extracted after chemical treatment (locality B-8 in Fig. 6).

4. Sandstones proximal to those from member 2, locally alternating with siltstones. Up to 50% of the member is made up of olistostrome, breccia, and conglomerate lenses a few meters thick and a few tens of meters long. Coarse-grained facies involve marbleized or, sometimes, oncolitic limestones, dolomites, and silicilites; more rarely, micritic light-gray limestones of variable roundness, and

well-rounded oval pebbles of tonalites and polymictic gritstones. The micritic limestones contain archeocyates. *Archaeocyathus erbiensis* Zhur., *Tegerocyathus* sp., which are typical representatives of early Cambrian fauna and indicate the Lower Cambrian Obruchev horizon (Volkov, 1966, Bondarenko, 1976), and *Irinacyathus* (?) cf. ratus (Vologdin), typical of the Botomian and Toyonian Stages of the upper half of the Lower Cambrian (Gusev and Kiselev, 1988), were also found in other sections (near Aktash village) among limestone clasts of olistostromes and conglomerates. Fragments of some lenses display a sort of zoning, the largest olistoliths being located in the center, haloed by smaller clasts. The olistoliths, composed mainly of Baratal limestones, are either flat with radiating ends or oval bodies up to 20 m long.

5. Polymictic coarse-grained sandstones containing sparse gravel clasts, olistoliths, and <50 cm thick and 3–5 m long lenses of breccias and conglomerates. The member occurs in the immediate vicinity of the Chuya road.

The olistostrome complex is overlain by a thick (at least 1 km) sequence of polymictic and quartz-feldspathic sandstones and rhythmically-bedded silty sandstones (silts) with siliceous, argillaceous and calc-argillaceous mineralogy. The thickness of the sandstone beds is many tens of meters, and the flysch layers are from a few centimeters to a few meters thick. In places, the rhythms start with polymictic gritstones. The base of the variegated sequence locally involves carbonate-siliceous olistoliths and conglomerate lenses and interbeds. Limestone clasts in conglomerates and olistoliths at the bottom of the variegated sequence contain trilobites and brachiopods from the Middle Cambrian Mundybash horizon (*Olenoides* sp., *Kootenis* ex. gr. *elongata* Resser, *Kootenis ontoensis* N. Tchern., *Kootoniella statkowskii* (Schmidt.), *Amgaspidella* cf. *elongata* N. Tchern., etc.) as well as brachiopods *Nisusia pospelovi* Aks. and *Kutorgina amzassica* Aks. (Perfiliev et al., 1994).

The lilac and red layers of siliceous rocks, which bear sponge spicules, were sampled from the upper part of the olistostrome complex and from the lower part of the silty sandstone formation.

The greatest portion of sponge spicules sampled from localities B-8 and 519 have very thick and strong hexactinic thorns. They should be attributed to the species *Cjulanciella asimmetrica* Fedorov, first described within the Middle Cambrian Amgaian Stage (the lowermost of the Amgaian trilobite zones is the Oryctocara regional zone) of the Kuonamka Formation in the Siberian Platform. An equivalent sponge spicule taxon was found in jasperic interbeds in a Middle Cambrian greenstone belt near Melbourne in eastern Australia. The siliceous rocks from locality 519 also contain rare fossils of sponge spicules *Disparella* cf. *fusiformis* Fedorov. This taxon was found among both Middle Cambrian (Kuonamka Formation, Oryctocara zone) and Upper Cambrian (Ogon'or Formation, the youngest Cambrian trilobitic layers of Parabolinites levis) layers on the Siberian Platform (Fedorov et al., 1987). It is noteworthy that the Ogon'or formation spans as much as the upper and middle Mayaian Stage of the Middle Cambrian and the whole Upper Cambrian. Locality 519 is stratigraphically higher than locality B-8 and, hence, must be younger. Thus, the rocks from locality B-8 can be dated as Middle Cambrian, and those from locality 519 as upper Middle to late Cambrian. Taking into consideration the Amgaian (lower Middle Cambrian) age of trilobite and brachiopod fossils in carbonate pebbles (Perfiliev et al., 1994), the rocks in locality B-8 can be considered as the uppermost Middle Cambrian and those in locality 519 as the latest Middle to Upper Cambrian. The paleontological constraints on stratigraphy of jaspers from the Chibit olistostrome and variegated silty sandstone formations provide a basis for dating the two stratons.

It is interesting to note that Lower Cambrian (Tommotian) archeocytes were found in limestone blocks among olistostrome accretionary mélange in the western Primorye region, and uncertain microfossils and sponge spicules were extracted from siliceous olistoliths (Gusev and Khalitova, 1988). The latter involve varieties with their shapes proximal to the spicules representative of *Cjulanciella* and *Disparella* genera.

Figure 6 shows cross-sections through the olistostrome complex in southeastern Gorny Altai compiled by different authors. The olistostrome horizons and lenses, and the olistoplaques are unevenly distributed throughout the sequence, which is in places more than 500 m thick. This attests to intricate facies transitions on the Anui-Chuya basin periphery. The lowermost strata of the olistostrome complex involve clastic material (olistoliths and olistoplaques or carbonate boulders and pebbles) transported chiefly from the accretionary complex, as well as rounded gabbroic and volcanic boulders and pebbles and polymictic sandstones brought from the island arcs. The coarse-grained clastics in the upper unit of the olistostrome complex are of island arc, accretionary-wedge and continental provenance. They are: polymictic sandstones along with gabbro, volcanic, and pyroxenite-like boulders and pebbles; basaltic clasts from oceanic islands, as well as olistostromes, possibly, serpentinites and amphibolites; and quartz-feldspathic sandstones, fragments of potassic granites and greenschists, apparently, from the Teletskoe metamorphic complex, respectively.

Petrographical studies for sandstones (Buslov, 1992; Buslov et al., 1993; Gusev and Kiselev, 1988; Gusev and Khalitova, 1988; Zybin, 1985) evidences sediment-transportation from the pre-Middle Cambrian units. They are most probably accretionary complex, the pre-Middle Cambrian Uimen-Lebed' primitive island arc, the Cambrian island arc and the metamorphic rocks (probably late Riphean Teletskoe complex). In this respect, the section is arranged as follows: the late Cambrian silty sandstone formation has a base composed of polymictic sandstones from an eroded island arc and quartz-feldspathic sandstones from its continental basement. The uppermost strata of the Gorny Altai Group comprise quartz-feldspathic sandstones, which attests to deep erosion of the island arc, whereby its continental basement became exposed, and the accretionary complex became buried beneath the deposits filling the Anui-Chuya basin.

Kurai Accretionary Wedge (Pre-Middle Cambrian): Structure and Composition

The Kurai accretionary wedge (Figs. 4, 5) is located north and east of the Anui-Chuya basin described above. It has been thoroughly studied in recent years. This part of the Gorny Altai is well exposed and accessible. The fragments of an early Caledonian accretion-collisional zone is believed to have been well preserved there. Boulders similar to the accretionary wedge origin are found in the Middle–late Cambrian Anui-Chuya basin. The terranes and their separating sutures are broken by late Paleozoic transverse intra-continental strike-slip faults and oblique thrusts as shown in figure 3.

The Kurai accretionary wedge is composed of the tectonic sheets of the Baratal seamount of variable composition and size, including oceanic sediments and basaltic units and seamount rocks, Chagan-Uzun oceanic ophiolites, and serpentinitic mélange with sheets and minor blocks of eclogite, garnet amphibolite and barroisite-actinolite schists. The barroisite-actinolite schists often occur within the accretionary prism as separate lenses. All the above-noted sheets and blocks are associated with the pre-Middle Cambrian olistostrome. In the Middle–late Paleozoic, the accretionary prism was folded. Its structural elements dip in the direction opposite to the late Paleozoic nappe-sheeted structure of the Kurai range, i.e., to the SW.

The accretionary prism consists of the three units divided into upper, intermediate and lower structural units with SW-dipping structure (Fig. 5).

(1) *The 15 km wide and 12 km thick upper structural unit* is composed of tectonic sheets dipping at 70–80° to the SW. The tectonic sheets and lenses consist of paleoseamount siliceous-limestone and carbonate rocks, olistostrome units (including olistoliths), and dark-gray or black limestone. The Baratal seamount is composed of two types of rocks: (a) Light-gray and gray rhythmically layered brecciated limestones. In places, some layers consist of gray cherts, siliceous shales, volcaniclastic rocks and primary and secondary hyaloclastic rocks. Those sediments were deposited close to active volcanoes, possibly at the bottom of their sub-water slopes, because they contain numerous fine fragments of clinopyroxene, orthopyroxene and hornblende of igneous origin. (b) Reef gray limestones and dolomites once composed tops of oceanic islands. The dark-gray and black limestones are different from paleoseamount carbonate rocks: they are of massive texture and contain H_2S with thin interbeds and lenses of black siliceous rocks. The black limestones contain the fragments of garnet, tourmaline, sillimanite, staurolite and corundum from metamorphic rocks. The dark-gray and black limestones may represent an exotic block, which was transported into the subduction zone together the crust of the Paleo-Asian ocean. There are no appropriate rocks for isotope dating, but Uchio et al. (2001) determined the 577±100 Ma age from the basement limestones by Pb–Pb method.

In the base of the upper structural unit there is a 3 km thick package of sheets composed of carbonate and polymictic olistostrome, siliceous rocks and unevenly metamorphosed volcanogenic-sedimentary rocks. Large olistoliths of up to tens of meters are found in the polymictic olistostrome as blocky segments with subordinate amount of tectonized matrix. The olistoliths are basalts, volcaniclastics, siliceous rocks and various limestones. Besides the sand-clay calcareous matrix, the olistostrome sequence includes sand-shale horizons containing well-rounded pebbles of marble-like limestone, dolomite, amygdaloidal-andesitic basalt and diabase porphyrites which could have been transported into the sedimentation basin from an island arc.

The sheets of siliceous rocks may reach many hundreds meters in thickness. They are composed of gray and dark-gray massive or rhythmically layered rocks. The thickness of a rhythm can reach 5 cm. Angular-clastic rocks, cemented by silica-rich material are found at the base of the rhythmic sequence. The clastic rocks are overlain by fine-grained gritstones and bedded cherts.

(2) *The intermediate structural unit* – the Arydzhan package of sheets, consists of four subunits, i.e., (a) basaltic series (oceanic island basalts - OIB and MORB), (b) volcanogenic-sedimentary sequence, (c) olistostrome and (d) metamorphic rocks (Gusev, 1991; Buslov et al., 1993). In places, the volcanic, volcanogenic-sedimentary rocks and olistostrome compose EW-trending folded sheets of variable size.

Table 1. XRF bulk analyses of magmatic and metamorphic rocks of the Baratal terrane.

	1	2	3	4	5	6	7	8	9	10	11	12	13	14	15	16	17	18	19	20	21	22
Sample	S1	S2	92-T-1	92-T-2	92-T-3	92-T-4	92-T-5	730	12048-4	586	157	621	621 a	2863	2865-1	2864-1	529-4	8523-1	905	904	907	B-96
SiO_2	48.43	49.53	48.99	49.16	47.07	48.69	48.87	49.67	48.9	49.2	49.67	47.6	44.1	46.89	50.13	48.25	46.75	48.05	48.46	47.39	51.14	50.15
TiO_2	1.68	1.54	1.008	1.096	1.034	1.14	1.129	1.51	3.25	1.18	2.13	2.23	2.4	2.15	1.64	2.17	1.54	2.08	1.99	1.96	1.73	1.51
Al_2O_3	13.8	14.94	14.9	15.07	15.23	15.5	15.48	13.73	13.91	14.75	13.66	13.3	12.9	13.62	13.44	13.26	10.93	13.61	12.5	13.88	12.56	14.56
Fe_2O_3	3.87	3.25	11.97	12.12	12.7	12.12	13.01	2.12	9.26	4.98	2.73	3.15	3.45	3.29	4.67	4.75	3.11	4	2.76	4.34	3.06	13.76
FeO	8.07	8.97						9.48	5.47	5.9	8.76	11.47	12.55	11.49	8.39	10.46	10.39	10.31	12.18	9.41	9.7	
MnO	0.21	0.2	0.15	0.14	0.17	0.15	0.16	0.2	0.2	0.19	0.26	0.24	0.29	0.23	0.2	0.23	0.21	0.17	0.14	0.24	0.24	0.26
MgO	5.67	5.17	5.71	5.78	6.73	6.09	6.46	6.75	3.63	7.23	7.81	6.53	7.67	6.95	6.85	6.65	11.14	6.84	8.7	6.95	6.58	3.89
CaO	9.83	7.16	9.99	9.97	9.58	9.44	6.88	9.36	5.38	7.13	8.36	10.42	10.18	10.14	9.84	8.72	7.86	9.25	8.75	12	10.29	5.44
Na_2O	2.9	4.03	2.87	2.74	2.98	3.06	3.75	2.9	4.1	3.8	2.8	2.2	2.4	1.75	2	2.09	2.86	3.3	2.14	1.64	1.81	5.76
K_2O	0.26	0.68	0.18	0.1	0.09	0.1	0.14	0.32	1	0.44	1.4	0.22	0.17	0.33	0.3	0.23	0.14	0.17	0.34	0.24	0.8	0.71
P_2O_5	0.16	0.27	0.113	0.118	0.112	0.11	0.116	0.15	0.6	0.14	0.17	0.23	0.19	0.17	0.11	0.14	0.15	0.15	0.16	0.2	0.14	0.58
LOI	4.98	3.82	4.02	4.15	3.92	3.92	4.08	3.12	4.71	3.89	2.99	2.08	3.46	2.97	1.94	2.14	3.63	2.01	2.69	2.42	2.41	3.86
Total	99.86	99.56	99.9	100.45	99.62	100.32	100.07	99.31	100.41	98.83	100.74	99.67	99.76	99.98	99.51	99.09	98.71	99.94	100.81	100.67	100.46	100.48
FeO/MgO	1.42	1.74						1.40	1.51	0.82	1.12	1.76	1.64	1.65	1.22	1.57	0.93	1.51	1.40	1.35	1.47	

Note: 1-2–oceanic crust 3rd layer basalts (23 samples), 3-7–oceanic pillow-lavas, 8-11–oceanic island pillow-lavas, 12-22–barroisite-actinolite schists.

Table 2. XRF bulk analyses of magmatic and metamorphic rocks of the Chagan-Uzun massif.

	1	2	3	4	5	6	7	8	9	10	11	12	13	14	15	16	17	18	19	20	21	22	23	24
Sample	C-101b	C-102b	C-102c	C-103c	C-104c	1458	1461	12787	Chu-3	Chu-4	Chu-6	Chu-7	C16a-91	Ch-11	Ch-915	Ch-916	C-965a	965a	Ch-13	Ch-14	Ch-915	Ch-916	Ch-917	Ch-919
SiO_2	51.6	51.27	47.17	50.69	51.4	52.43	50.73	53.91	46.69	47.37	48.66	48.31	47.89	45.29	47.1	47.88	45.02	45.93	44.48	46.86	47.1	47.88	47.36	46.55
TiO_2	1.46	1.38	1.65	1.44	1.42	0.86	1.17	1.08	1.8	1.61	1.84	1.54	1.61	2.28	2.17	2.22	2.42	2.99	2.12	1.85	2.171	2.218	2.17	1.586
Al_2O_3	14.03	13.95	14.6	13.88	14.02	23.45	16.9	16.2	14.03	12.72	12.87	11.84	13.67	13.14	13.13	12.39	13.81	13.64	14.17	13.52	13.13	12.39	13.58	14.06
Fe_2O_3	14.96	14.59	16.42	14.8	14.68	2.87	8.69	9.51	14.24	13.28	15.22	14.47	13	17.66	15.12	15.04	16.6	15.75	16.04	14.68	15.12	15.04	15.29	13.23
MnO	0.24	0.23	0.24	0.22	0.23	0.19	0.21	0.19	0.25	0.24	0.23	0.24	0.22	0.35	0.23	0.25	0.15	0.28	0.29	0.22	0.234	0.249	0.286	0.22
MgO	4.2	4.19	4.88	4.34	4.21	6.15	6.75	5.04	7.6	7.78	6.88	8.75	7.18	8	6.93	6.71	7.09	6.43	7.79	7.74	6.93	6.71	7.45	7.52
CaO	7.11	7.88	8.71	7.95	7.85	7.99	9.11	7.15	8.56	11.08	7.27	10.09	10.69	6.96	9.22	9.24	10.87	10.1	10.52	9.39	9.22	9.24	8.29	10.36
Na_2O	6.01	4.21	4.18	4.69	5.02	3.52	3.42	3	4.06	3.54	4.09	3	2.89	3.15	3.95	3.29	2.51	2.07	2.52	3.51	3.95	3.29	3.49	3.4
K_2O	0.54	0.32	0.37	0.32	0.4	0.34	0.37	0.9	0.23	0.08	0.18	0.08	0.13	0.34	0.26	0.28	0.33	0.25	0.36	0.18	0.26	0.28	0.22	0.15
P_2O_5	0.13	0.13	0.16	0.13	0.13	0.08	0.12	0.12	0.15	0.11	0.18	0.08	0.16	0.18	0.17	0.21	0.21	0.19	0.13	0.16	0.174	0.205	0.162	0.19
LOI	0.48	0.78	1.34	1.04	0.48	2.97	3.25	3.1	2.08	2.34	1.94	1.48	2.46	2.54	1.38	1.87	3.18	3.47	1.7	1.2	1.38	1.87	0.94	2.48
Total	100.28	98.15	98.38	98.46	99.36	97.88	97.47	97.1	97.61	97.81	97.42	98.4	97.44	97.35	98.28	97.51	99.01	97.63	98.42	98.11	98.29	97.50	98.30	97.27

Note: 1-5–island arc dykes, 6-16–amphibolites from metamorphic sole, 17-24–eclogites and garnet amphibolites.

(a) The basaltic sequence is dominated by dark-gray and gray-green pillow-lavas and variolitic lavas, and also includes minor amounts of amygdaloidal sub-alkaline basalts, diabase and gabbro-diabase dykes and sills (Table 1). The lavas are metamorphosed to the low-temperature greenschist facies. The magmatic rocks are associated with sparse interlayers and lenses of dark-gray and gray clastic limestone, dolomite, black and gray siliceous rocks and rare sandstone. (b) The volcanogenic-sedimentary sequence is mainly composed of dark-gray or reddish reef limestones of layered and massive fabric interbedded with green-gray chlorite-bearing shales and volacaniclastic sandstones. (c) Clastic composition of olistostromes is variable. The olistostromes were formed in two stages: the entrance of the seamount into the trench and the collapse of the frontal part of the Baratal terrane during its subduction. There are two main types of olistostrome: siliceous-limestone-basaltic and polymictic. Gritstones and breccias compose the matrix of the first type olistostrome. There are fragments of gray, light-gray and black cherts and red jasper and smaller amounts of basalt, carbonate, and thin-layered carbonate shales. The gritstones and breccias are cemented by siliceous and carbonate-siliceous rocks and shales and contain olistoliths of mainly siliceous composition with minor basalts and carbonates. The siliceous olistoliths are composed of black and gray chert and red jasper. They are of flat or angular shape, up to several tens of meters thick and hundreds of meters long. Their clastic material could result from disintegration of a silica-rich volcanogenic-sedimentary sequence. Such a sequence could form in a seamount-bottom environment. The polymictic olistostrome consists of sandstone, clay, clay-marl and andesitic tuff matrix and clastics of variable size. Olistoliths comprise siliceous rocks, limestone, dolomite and basalt. (d) Metamorphic rocks are greenschist, amphibolite, and garnet amphibolite. The metamorphic sequence contains two sheets of crystalline schists (garnet amphibolite and amphibolite) dipping westward at a 70° angle which ranges in thickness from 50 to 250 m by strike. Ota et al. (2000) established four progressive metamorphic zones, although amphibolites show the traces of diaphthoresis and mélange processes. Fresh garnet amphibolite contains zoned garnet with poikilitic quartz, amphibole, and titanite. The amphibolites and garnet amphibolites possess chemical characteristics of normal-type mid-oceanic ridge basalt (N-MORB) (Tables 2, 3; Fig. 8).

(3) *The 3 km thick lower structural unit* – the Chagan-Uzun sheeted-mélange zone underlying the upper and intermediate units. There are two types of sections: (a) South of Kurai village, the Chuya left bank, the zone is composed of polymictic and serpentinitic mélanges. The

Table. 3. REE and RE in magmatic and metamorphic rocks of the Baratal terrane (NAA).

	1	2	3	4	5	6	7	8	9	10	11
Sample	92-T-4	92-T-2	965A	Ch-912	Ch-916	Ch-917	Ch-919	B-902	B-904	B-905	B-907
La	2.5	2.8	4	3.2	5.3	3.9	3.3	1.2	5.3	5.5	4.5
Ce	6	6	13	10	18.5	15.6	8.5	3.5	13.5	15.8	9.2
Nd	8	6.2	13	7	12.6	13	9	39	10.9	13.8	9
Sm	2.4	2.2	4.9	3.4	5.5	4.6	3.6	1.1	3.6	3.9	3.6
Eu	1.15	1.1	1.9	1.3	2	1.5	1.6	0.46	1.73	1.14	1.25
Gd	3.8	3					3.2	2.1	5.5	5.2	3.7
Tb	0.65	0.58	1.4	0.88	1.35	1.25	0.9	0.3	0.9	0.94	0.7
Dy	3.6	5	7.5	5.8	6.7	6	5.6				
Tm								0.3	0.7	0.72	0.4
Yb	2.5	2.7	5.6	4	7.5	5.4	4.7	1.6	4.2	4.3	3.6
Lu	0.48	0.42	0.88	0.62	1.2	0.9	0.9	0.3	0.68	0.63	0.48
Sc	30	36	45	52	62	57	57	49	56	55	49
Hf	1.3	1.6	5.3	3	5.2	3.5	2.5	0.3	0.7	0.47	0.7
Ta	0.1	0.12	0.3	0.2	0.35	0.3	0.15	0.04	0.19	0.17	0.11
Th	0.15	0.2	1.7	0.4	0.9	0		0.75	29	3.7	2.4
							Fe	7	10	11.5	10
							Cr	190	135	110	90
							Co	35	42	48	41
							Ni	3.3	1.24	2	1.54
							Zr	13	108	11	89
							Nb	1.8	5	5	5
							Y	9.5	29	26	24
							Rb	9	4	6	12.1
							Sr	250	328	137	153
							Ba	220	110	120	206

Note: Chondrite normalizing values: La=0.31, Ce=0.808, Nd=0.60, Sm=0.195, Eu=0.0735, Gd=0.259, Tb=0.0474, Yb=0.209, Dy=0.322, Tm=0.0324, Yb=209, Lu=0.0322, 1-2–oceanic pillow-lavas (Taldy-Tyurgun), 3-5–eclogites and Ga-amphibolites after oceanic basalts, 6-7–metamorphic sole, 8-11–garnet amphibolites and barroisite-actinolite schists.

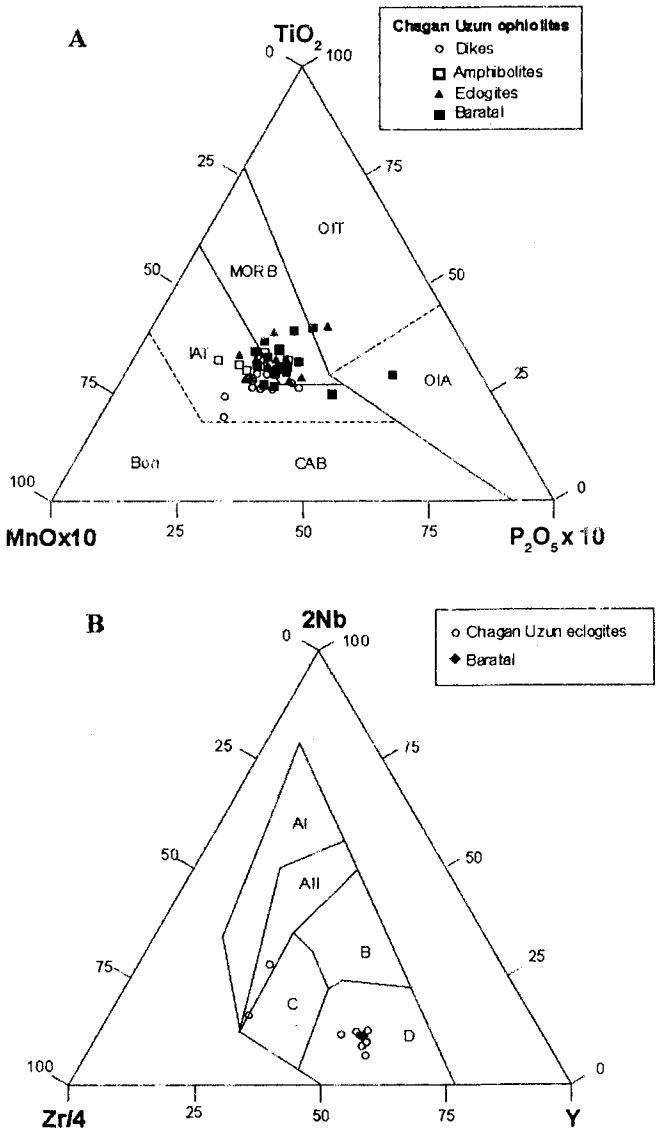

AI - within-plate alkaline basalts, AII - within-plate alkaline basalts and within-plate tholeiites, B - E-type MORB, C - within-plate tholeiites and volcanic-arc basalts, D - N-type MORB and volcanic-arc basalts (Meschede, 1986).

Fig. 8. Geochemistry of rocks: (A) - the MnO-TiO_2-P_2O_5 discrimination diagram of Baratal basalts and Chagan-Uzun basic rocks. The fields are MORB, OIT–ocean-island/seamount tholeiite, OIA–ocean-island/seamount alkali basalt, CAB–island arc calc-alkaline basalt, IAT–island arc tholeiite, Bon–boninite. (B)- the Zr/4-2Nb-Y diagram for Baratal basalts.

polymictic mélange includes up to several meters long blocks of serpentinized pyroxene-olivine porphyrite, diaphthorized garnet amphibolites with relic eclogite, and amphibolites and matrix consisting of serpentinite schists and mylonites after metamorphic rocks and basalts. The serpentinitic mélange consists of foliated serpentinite incorporating blocks of massive serpentinite and light-gray cryptocrystalline rodingite. The serpentinite bodies, up to several meters long, extend over a distance of many kilometers parallel to the NS-trending Arydzhan sheeted zone. (b) Near Chagan-Uzun village, the Chuya left bank, the intermediate structural unit and a sheeted-mélange zone consist of (S→N, downsection):

Intermediate structural unit

1. The siliceous-carbonate nappe of Baratal seamount is exposed as several deformed steptoes. Its visible thickness reaches first hundreds of meters. In their basis there is a tectonic mélange consisting of greenschist matrix, fine fragments and blocks of limestones and cherts.

2. A sheet of metabasalts of some tens to hundreds of meters thick composed of schists, boudins and lenses.

3. A several meters thick olistostrome is composed of the rocks, which underwent cataclasis and are interbedded with siliceous-carbonate gritstones, siliceous shales and marl shales. The fragments are poor-graded dolomites, limestones and cherts up to several centimeters in diameter.

Sheeted-mélange zone

4. The upper sheet of Chagan-Uzun ophioliote massif is made up of ultrabasics: fresh peridotites in the upper horizon and massive serpentinites in the lower horizon. The sheets of serpentinitic mélange up to 100 m thick, contain the inclusions of massive serpentinites, eclogite-garnet amphibolites and minor greenschists. The largest bodies are composed of garnet amphibolites containing eclogite relicts. The lenses and interlayers of cherts are found in metamorphic rocks. The eclogite have undergone high-pressure greenschist diaphthoresis, which is regularly exhibited at the marginal parts of bodies. The samples, a series of rocks from greenschist diaphthorites (with relics of garnet) to garnet amphibolites (with relics of eclogite), were selected with a 10–15 m interval at the upper metamorphic sheet of the section along the route (south to north). Bulk chemistry and trace element concentrations for these samples are cited in tables 1–3.

5. The lower sheet of Chagan-Uzun massif is composed of massive and schistose serpentinites which contain the boudins and deformed dykes of gabbro and gabbro-diabases. The outside zones of these bodies are made up of rodingites. Below, there are rocks with geochemical characteristics of oceanic island basalts (Buslov et al., 1993). At the contact we can clearly see the metamorphic sole of the Chagan-Uzun massif composed of garnet-free amphibolites. Its thickness reaches some hundreds of meters. Far from the contact, the amphibolites gradually pass into the well-known basaltic porphyrites.

The eclogitic rocks from the sheeted-mélange zone are of special interest. Eclogite-amphibolite and garnet

amphibolite bodies are found in the mélange of the third zone. Up to 4–5 m wide and 10 m long eclogite-amphibolite bodies consist of eclogite bands alternating with garnet amphibolites, which are also composed of their apical parts and up to several centimeters thick transverse narrow zones. In several bodies eclogites have been preserved as small lenses in garnet amphibolite. Up to 30 m wide and 200 m long garnet amphibolite bodies underwent the greenschist diaphthoresis developing along the marginal parts of the sheets.

The main rock-forming minerals in eclogitic rocks are Ca-almandine, omphacite and amphiboles of the glaucophane group (Buslov and Watanabe, 1996). Well-faced Ca-almandine is 0.1 to 0.3 cm in diameter with fine vortex-arranged inclusions of glaucophane, winchite, titanite and apatite. The garnet grains are cemented by isometric omphacite grains up to 0.1 cm in diameter, which locally compose narrow bands. Some of garnet and omphacite crystals are rimmed by Ca-Na amphiboles of the winchite-barroisite group. Zonal amphibole grains are 0.2–0.3 cm long. Glaucophane is rimmed by barroisite and actinolite, or winchite is rimmed by actinolite/barroisite (Table 4). The relationship between eclogite and garnet amphibolite, however, must be examined in detail. Under the microscope, we discriminate at least two kinds of garnet amphibolites with and without clinopyroxene as shown in figure 9. Clinopyroxene in the amphibolite is always rimmed by dark and fine-grained materials, suggesting partial breakdown of clinopyroxene (Fig. 9a, b). Amphibole is barroisite in some cases, but often heterogeneous (zoned amphibole). The protolith may have been barroisite/glaucophane eclogite. Garnet is finely fractured, but exhibits progressive zoning pattern represented by increasing MgO (1.55–2.21%) and decreasing MnO (1.67–0.40%). Although a marginal part of the garnet does not exhibit distinct decomposition by retrogressive metamorphism, the inner part of the garnet (high Ca garnet) is broken down into fine-grained mineral assemblages composed mainly of epidote. Retrograde recrystallization shown by zoned amphibole or veining is always observed.

Garnet amphibolite without clinopyroxene is texturally different from eclogitic garnet amphibole in typical cases. Garnet with spiral or concentric inclusions exhibits nice euhedral morphology (Fig. 9c, d) and amphibole is homogenous. Our preliminary K–Ar dating for eclogitic garnet amphibolite (Fig. 9a, b) yielded early Cambrian age, but the influence of retrograde metamorphism was obvious. Therefore, we obtain Ar–Ar geochronological dates (the analyzed amphibole specimens 124-3, 124-4,

Table 4. Microprobe analyses of Ca-Na amphiboles from Chagan-Uzun metamorphics. C: Core, R: Rim. Preliminary K–Ar dating for amphibole of 965a , which includes heterogeneous amphibole result from retrogressive metamorphism, is 535 Ma. As shown in figure10, Ar–Ar data indicate influence of later thermal episodes. Sample 124-b, however, contains homogeneous barroisite and has a plateau age 635 Ma.

	124-3a			124-3b			124-4		
No.	R1	C	R2	R1	C	R2	R1	C	R2
SiO_2	48.67	55.36	50.53	45.38	44.72	47.04	49.01	55.76	49.88
TiO_2	0.32	0.07	0.18	0.83	0.73	0.38	0.22	0.02	0.23
Cr_2O_3	0.12	0.29	0.04	0.31	0.77	0.21	0.03	0.02	0.02
Al_2O_3	10.44	10.88	9.35	13.23	13.1	11.3	10.19	9.12	9.00
FeO	14.76	12.65	14.43	15.26	15.24	14.38	14.22	13.84	14.75
MnO	0.01	0.01	0.03	0.02	0.019	0.01	0.02	0.10	0.02
MgO	11.03	9.05	9.94	9.81	9.57	10.70	10.83	9.66	11.34
CaO	7.75	2.05	7.14	8.4	8.41	8.08	7.34	3.50	7.92
Na_2O	3.94	6.03	3.60	4.18	4.21	3.91	4.06	5.18	3.56
K_2O	0.27	0.06	0.20	0.23	0.22	0.38	0.25	0.05	0.25
Total	97.31	96.44	95.44	97.65	96.99	96.38	96.16	97.25	96.97
Si	7.30	7.86	7.64	6.88	6.84	7.16	7.40	7.97	7.5
Ti	0.04	0.01	0.02	0.09	0.08	0.04	0.02	0.00	0.03
Cr	0.01	0.03	0.00	0.04	0.09	0.03	0.00	0.00	0.00
Al	1.85	1.82	1.67	2.36	2.36	2.03	1.81	1.54	1.59
Fe^{3+}	0.00	0.00	0.00	0.00	0.00	0.00	0.00	0.00	0.00
Fe^{2+}	1.85	1.50	1.82	1.93	1.95	1.83	1.79	1.65	1.85
Mn	0.00	0.00	0.00	0.00	0.00	0.00	0.00	0.01	0.00
Mg	2.47	1.92	2.24	2.22	2.18	2.43	2.44	2.06	2.54
Ca	1.25	0.31	1.16	1.36	1.38	1.32	1.19	0.54	1.28
Na	1.15	1.66	1.05	1.23	1.25	1.15	1.19	1.43	1.04
K	0.05	0.01	0.04	0.05	0.04	0.07	0.05	0.01	0.05
Ca/K	50.26	57.26	60.91	62.43	65.60	37.31	51.67	114.36	54.86
Sum	15.96	15.13	15.64	16.16	16.19	16.06	15.89	15.21	15.88
Mg#	0.57	0.56	0.55	0.53	0.53	0.57	0.58	0.55	0.58
	Barroisite	Glaucoph	Winchite	Barroisite	Barroisite	Barroisite	Barroisite	Winchite	Barroisite

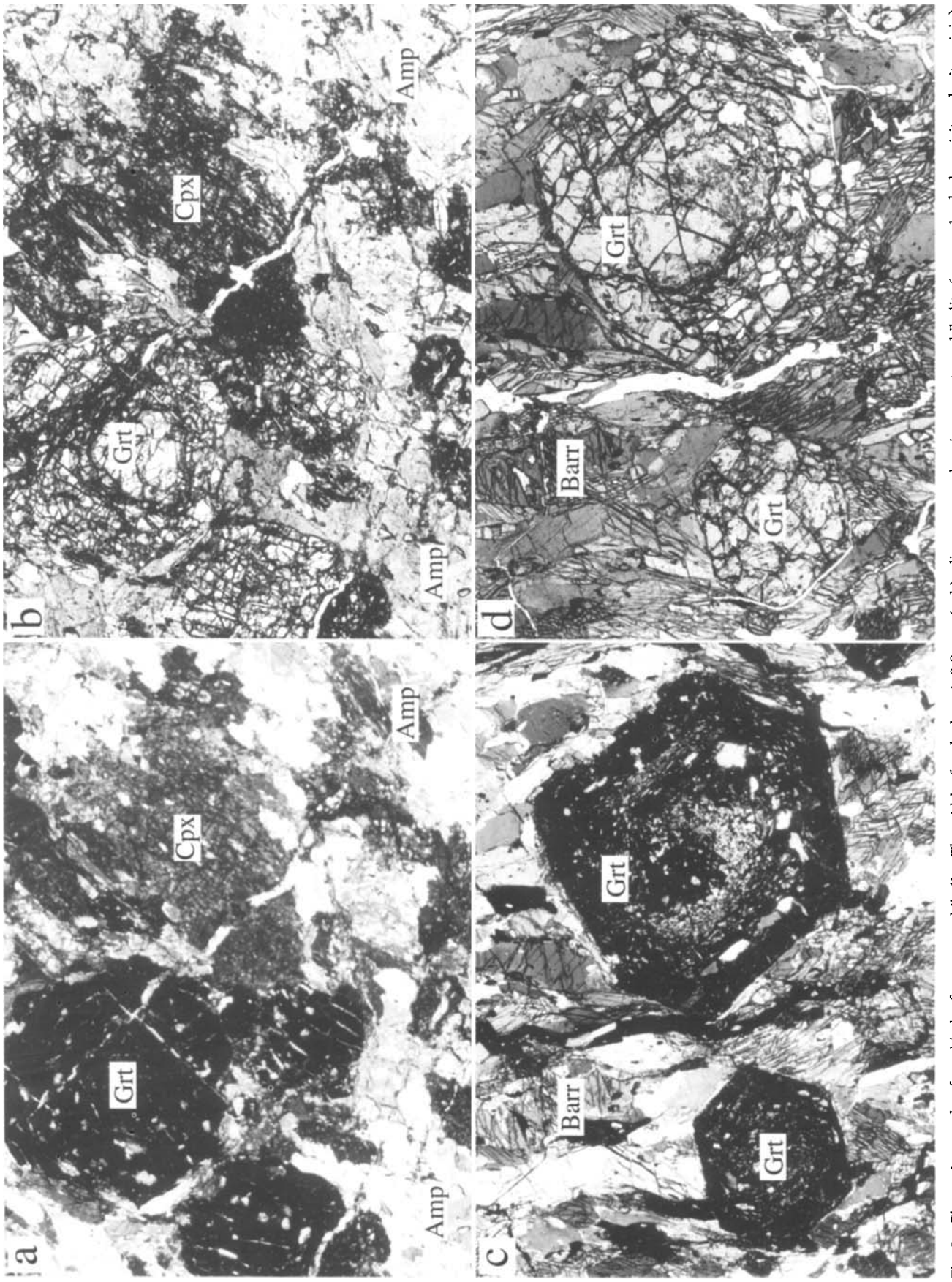

Fig. 9. Photomicrographs of two kinds of garnet amphibolite. The width of each photo is 0.9 mm. (a, b): clinopyroxene bearing garnet amphibolite (assumed to be barroisite eclogite origin). Clinopyroxene decomposes fine-grained dark material and barroisitic amphibole is zoned. Retrogressive recrystallization such as fibrous, tiny actinolite surrounding clinopyroxene is often observed. (c, d): clinopyroxene free garnet amphibolite. Note euhedral garnet and homogeneous barroisite.

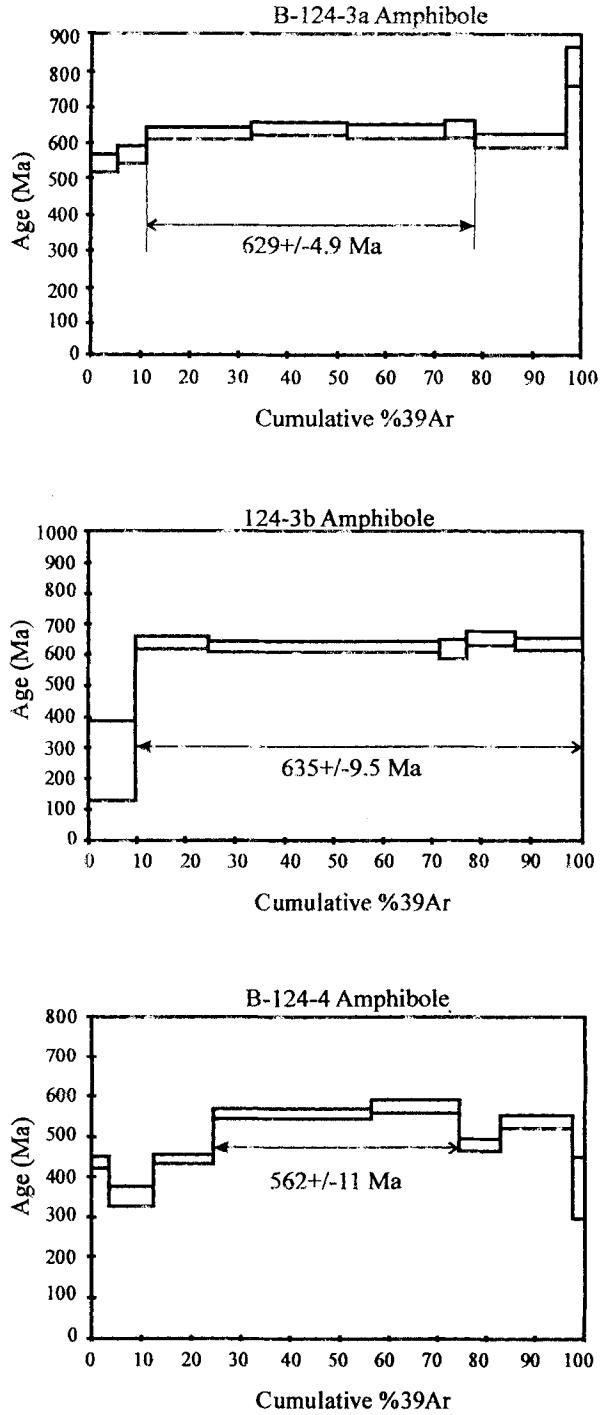

Fig. 10. Ar–Ar results for Chagan-Uzun eclogites (amphibole). Compare amphibole compositions in table 4. Ca/K ratios are 50.3–60.1 in B-124-3a, 37.3–65.6 in B-134-3b and 51.7–114.4 in B-124-4. The age for B-124-4 is meaningless.

and 124-5 of 627, 635 Ma (samples 124-3a and 124-3b), and 562 Ma (sample 124-4) (Fig. 10). All three indicate low temperature Ar loss which is consistent with a younger K–Ar age (early Cambrian). Although the plateau age is ca. 635 Ma, it may give an older age than real exhumation age due to correction for sample of very low K contents. Our preliminary study of garnet amphibolite from separate blocks without eclogitic facies indicates Ordovician K–Ar ages (ca. 470 Ma, ca. 480 Ma, Buslov and Watanabe, 1996), but the significance is still open to question. As far as the Ordovician rocks occur in the marginal part of the garnet amphibolite, their ages may reflect either a retrogressive stage, or formation of garnet amphibolite. The K–Ar phengite age of greenschists (garnet-phengite-chlorite-quartz-albite-titanite-calcite-opaque mineral, Akiyama, 1994) along the southern margin of the mélange unit is 567 Ma (Table 5). The greenschists contain garnets, but no biotite, indicating high-pressure metamorphism. Garnet (0.5 mm in diameter) in the schist shows a distinct retrogressive metamorphic episode. From the core to the margin MgO and MnO contents range from 1.19 to 0.62% and 1.61 to 8.97%, respectively. Taking into account the low closure temperature of mica, the age of 567 Ma may represent a later exhumation stage of high-pressure metamorphic rocks. Thus, we conclude that exhumation of eclogite with high-pressure greenschists occurred in Vendian. Later high-pressure metamorphism in Ordovician is uncertain. However, due to the presence of Ordovician high-pressure rocks in the Chara belt (see Fig. 1), we do not deny a possibility of Ordovicain metamorphism in the Chagan-Uzun massif during the collision stage.

Boudinated and deformed gabbro, gabbro-diabase, and diabase dykes cut the lower sheet and are compositionally close to the calc-alkaline island arc series of probably early to Middle Cambrian age. They record the formation of the Gorny Altai more evolved island arc. The metamorphic sole in the base of Chagan-Uzun ophiolites is composed of garnet-free amphibolites. A preliminary K–Ar amphibole age is 523 Ma (Buslov and Watanabe, 1996).

PT estimations for rock assemblages of the upper sheet, including eclogites, are 13–14 kbar and 620–700°C, i.e., they formed at a depth of 50–60 km, whereas meta-gabbro, rodingites and garnet-free amphibolites of the lower sheet, at 2–3 kbar (6–8 km depth) (Buslov and Watanabe, 1996). We suggest that the upper sheet with eclogites is an

Table 5. K–Ar age for micaceous fraction and chemical composition of mica of Chagan-Uzun metamorphic rock (greenschist) (Akiyama, 1994). HCl was not used for sample separation for a possible damage of low-temperature phengite. Low K may depend on the mixture of phengite and chlorite.

Sample No.	93062213		Rock type	Greenschist	
Mineral	Mesh size	K (wt.%)	Rad. Argon40 (10^{-6}ccSTP/g)	K–Ar age (Ma)	Non Rad Ar (%)
Phengite+Chl	150–200	2.67±0.05	6914.5±71.13	567.3±11.0	3

assemblage of subducted rocks, and amphibolites at the bottom of the lower sheet formed later – during the incorporation of hot ophiolites into the accretionary wedge or during their thrusting over oceanic floor basalts, like it was proposed for Oman ophiolites and other similar cases (Nicolas, 1989). The metamorphic rocks are cut by island arc gabbro-diabase dykes.

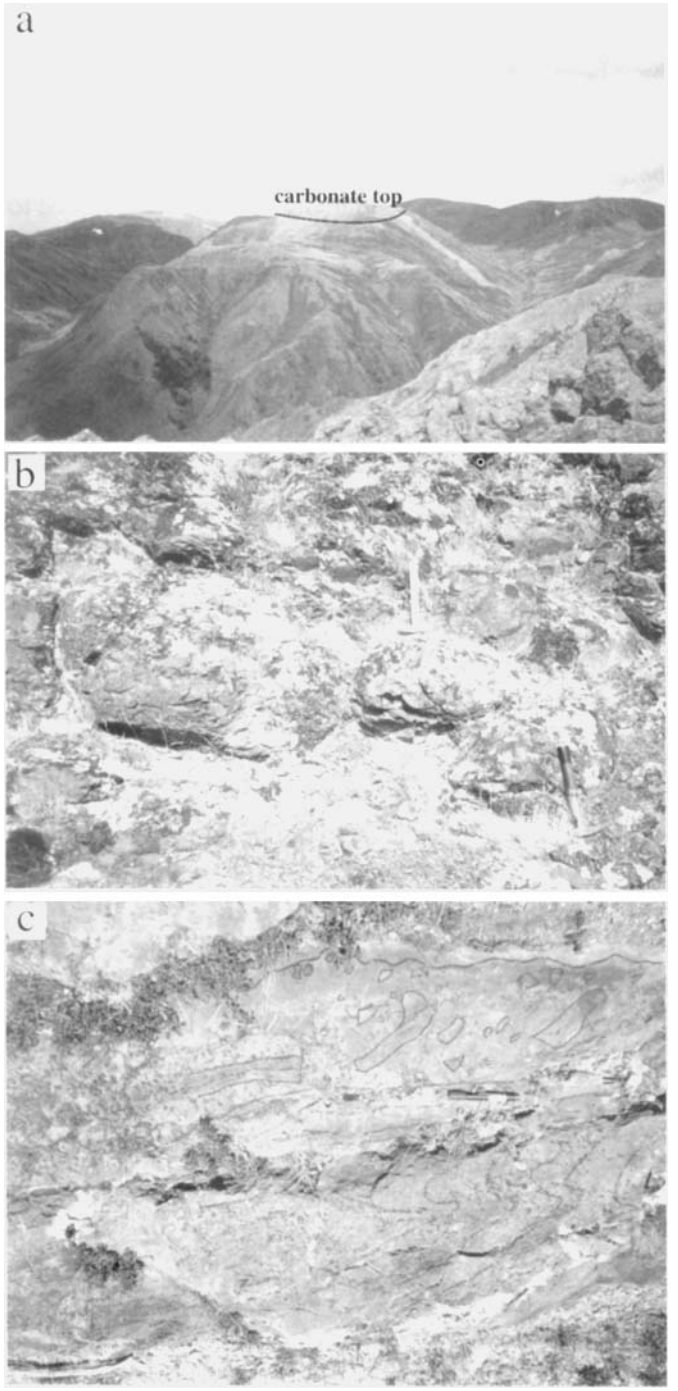

Fig. 11. (a) A photo of the contact zone between the carbonate top of an oceanic island and the lower sedimentary-volcanogenic unit. (b) A photo of outcropped pillow lavas. (c) A photo of carbonate clastic island-slope facies.

The Baratal paleoseamount is composed of laterally changing sedimentary facies of oceanic islands and their underlying basalts. We can reconstruct the upper oceanic island top units of predominantly carbonate composition and the lower sedimentary-volcanogenic units, as well as a lot of siliceous-limestone and clastic island-slope facies (Figs. 11a, b, c). The sheets of paleoseamount assemblages alternate with olistostrome sheets and lenses/fragments of an exotic terrane consisting of dark-gray-black sulphured-hydrogen limestones.

The bulk compositions of the Baratal volcanogenic and metamorphic rocks and Chagan-Uzun ophiolites are cited in tables 1 and 2. The major element chemistry of basalts shows that they all belong to the high-Fe tholeiitic basaltic series, the Fe/Mg ratio ranging from 1.47 to 4.06. In the $TiO-10MnO-10P_2O_5$ discrimination diagram (Fig. 8a), the compositional points of Chagan-Uzun island arc dykes, basalt-derived amphibolites and eclogites and Baratal pillow-lavas, oceanic crust basalts and basalt-derived metamorphic schists form a single area in the fields of MORB and island arc tholeiites. Rare-earth and trace element chemistry of Baratal rocks (Table 3) also indicates their close relation to oceanic ophiolites. The rocks are rather poor in LREE and their La/Yb ratio ranges from 0.7 to 1.28 indicating a weak enrichment in HREE (Table 3). In the Zr/4-2Nb-Y discrimination diagram (Fig. 8b) the points are mainly in the fields of N-type MORB/volcanic-arc basalts and within-plate alkaline basalts and tholeiites (Rollinson, 1993). The multi-component patterns of basalt-derived metamorphics of the Baratal terrane are close to those of N-MORB and support the idea that mainly mid-oceanic ridge ophiolites have been subducted and metamorphosed (Fig. 12).

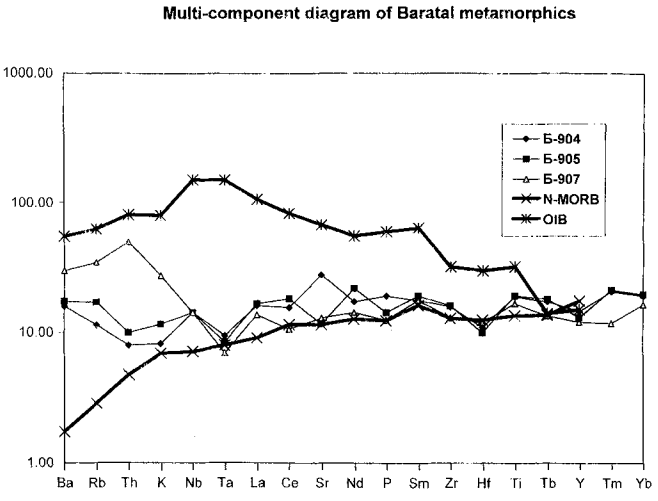

Fig. 12. Trace element concentrations in Baratal basaltic rocks normalized to the composition of the primordial mantle. The normalizing values and average N-type MORB and OIB concentrations are taken from Rollinson (1993).

In general, according to the structural position, rock assemblages, and major and trace element chemistry of the Baratal terrane can be regarded a seamount with a fragment of the oceanic crust at the base. In the earliest Cambrian, the Baratal terrane and the adjacent segments of the oceanic lithosphere (Chagan-Uzun ophiolites) were involved into the subduction and a part of rocks underwent a low- to high-grade metamorphism. In the latest early Cambrian, the Baratal terrane blocked the subduction zone and collided with the Kurai fragment of the Uimen-Lebed primitive island arc. The collision resulted in the generation of reverse flows in the accretionary wedge and rapid exhumation of the metamorphosed oceanic crust rocks – Chagan-Uzun ophiolites, eclogites and garnet amphibolites. Major and trace element chemistry of high-pressure metamorphic rocks is similar to MORB and OIB (Fig. 8).

Uimen-Lebed Island Arc

Its upper part (northern side) consists of Devonian epidote-amphibolite - amphibolite facies metamorphics, although the protoliths are estimated to be Precambrian. The metamorphic rocks are regarded as the Kurai metamorphic complex. The Kurai complex represents a tectonic nappe which is solely is composed of serpentinite schists and mélanges. Beneath this structural group there is a package of tectonic sheets comprising island arc ophiolite units: (1) a layered gabbro-pyroxenite complex, (2) sheeted-dyke complex, (3) dyke-sill complex, (4) volcanogenic unit. Besides, the nappe-sheeted structure includes calc-terrigenous rocks, black shales and turbidites. This terrigenous unit covers the ophiolitic unit and replaces it toward the marginal sea.

The primitive island arc units occur alternately with pre-late Cambrian more evolved island arc units, which consists of andesite, calc graywacke and volcanogenic turbidites. The gabbro-pyroxenite unit is found in two 1 km thick, gigantic tectonic sheets composed of serpentinite, wherlite, cumulative clinopyroxenite and layered gabbro. The layered unit is intruded by quartz diorite and plagiogranite dykes. The sheeted dyke and dyke-sill units are associated with volcanogenic-terrigenous rocks, such as diabase, gabbro-diabase, gabbro, and boninite series rocks. According to the previous geochemical studies, the volcanogenic assemblages include oceanic island and MORB tholeiites, MORB and island arc calc-alkaline volcanics and boninites (Table 6; Figs. 8, 12, 13) (Buslov et al., 1993; Simonov et al., 1994; Buslov et al., 1998). The chemistry of Uimen-Lebed boninites is close to the boninites of Tonga arc, Mariana arc, West Sayan and Khan-Taishirin in SiO_2, TiO_2, Al_2O_3, and MgO (Table 6). In the MnO-TiO_2-P_2O_5 diagram the Uimen-Lebed boninites and gabbro/basalts form a single trend (Fig. 12) . The main difference between Uimen-Lebed and western Pacific boninite is the composition of clinopyroxene (Simonov et al., 1994). The Uimen-Lebed boninites contains up to 1.5 cm long clinopyroxene phenocrysts, which are, along with other primary minerals, replaced by chlorite, epidote, actinolite, and clinozoisite (Buslov et al., 1997). Fresh grains of clinopyroxene, olivine and chromite are very rare. No orthopyroxene phenocrysts have been found yet. Microprobe analysis of clinopyroxene showed that it is represented by endiopside. Cr-spinel is compositionally close to that from the western Pacific boninites (Simonov et al., 1994).

The boninite-bearing ophiolites, which are assigned to be Vendian-Cambrian, are found in many sheets displaced along strike-slip faults in the present-day mosaic structure of Gorny Altai. Figure 1 shows the geographical and structural position of ophiolites in the Gorny Altai, West Sayan, East Sayan and western Mongolia. Taking into consideration the superimposed strike-slip deformations we can conclude that boninite-bearing ophiolites and marginal-sea units were structurally located between Vendian–early Cambrian accretionary units and late Riphean rock units.

Island arc ophiolites have a typical set of rocks specified by sheeted dyke complex. They provide evidence for the spreading of the oceanic crust under the subduction zone at the initial stages of ensimatic island arc evolution. Usually, well-preserved sections of island arc ophiolites

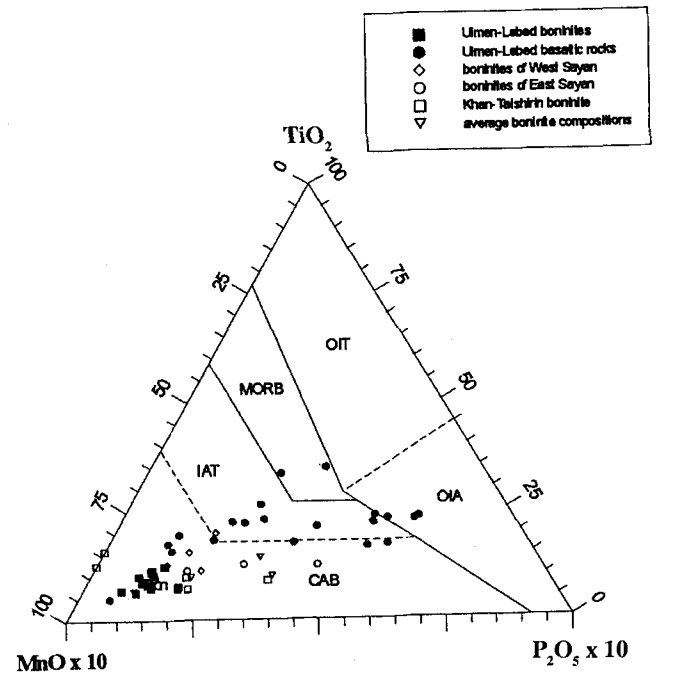

Fig. 13. The MnO-TiO_2-P_2O_5 discrimination diagram of Altai-Sayan-Mongolian boninites and associated basic rocks (the fields see in figure 8).

Table 6. XRF bulk analyses of Uimen-Lebed boninites and associated volcanics and gabbro.

	1	2	3	4	5	6	7	8	9	10	11	12	13	14	15	16	17	18	19	20	21	22	23	24	25	26
Sample	B-930	B-951	B-950	B-952	B-916	B-926	C-106a	C-106c	C-107B	C-13/1	C-13/3	C-54C	C-107a	C-110c	C-113B	C-113c	C-113d	C-113e	C-43	C-4a	B-t5	C-41	B-958	C-110B	C-111c	C-111d
SiO_2	51.95	54.25	52.33	55.44	54.69	53.92	57.13	56.90	56.38	57.90	58.78	50.12	50.55	51.63	52.12	52.10	49.15	48.85	52.97	49.71	53.12	67.06	57.08	55.47	55.60	57.61
Al_2O_3	15.66	15.36	9.10	11.86	8.35	12.23	11.78	11.67	9.71	11.82	12.50	9.21	16.71	15.99	14.64	14.69	15.58	15.80	17.42	19.21	19.24	16.42	17.83	13.66	16.14	16.63
TiO_2	0.35	0.31	0.19	0.38	0.24	0.21	0.24	0.25	0.35	0.33	0.35	0.20	1.33	1.30	3.06	3.07	2.72	2.48	0.86	0.47	0.64	0.61	0.94	1.25	1.43	1.35
P_2O_5	0.03	0.03	0.02	0.04	0.04	0.05	0.03	0.03	0.04	0.03	0.03	0.03	0.11	0.24	0.77	0.78	0.62	0.56	0.06	0.03	0.06	0.13	0.12	0.12	0.44	0.44
FeO*	9.34	10.90	9.19	10.74	10.49	10.03	9.94	10.35	10.07	10.33	10.21	17.66	16.38	13.91	13.28	12.60	13.54	13.34	14.08	9.43	10.08	7.26	12.33	14.93	11.55	11.34
CaO	11.26	8.04	12.83	9.03	9.65	12.94	8.24	7.69	10.09	4.60	2.44	10.57	3.63	12.70	6.56	6.61	6.64	7.98	7.57	10.60	5.20	2.48	3.50	4.46	4.27	2.72
MgO	8.31	7.80	14.36	9.72	14.41	9.31	10.67	10.65	10.55	13.58	13.70	11.59	7.17	3.42	5.37	5.46	6.31	6.82	3.70	7.22	4.87	1.00	3.52	3.97	4.93	4.25
Na_2O	2.59	2.76	1.29	2.18	1.24	0.98	1.18	1.98	2.22	1.10	1.64	0.34	3.83	0.55	3.90	4.35	4.88	3.46	1.90	2.11	6.21	4.12	4.18	5.84	5.31	5.32
K_2O	0.22	0.33	0.47	0.36	0.64	0.12	0.56	0.25	0.33	0.07	0.12	0.02	0.14	0.03	0.06	0.08	0.25	0.40	1.15	1.05	0.43	0.77	0.29	0.07	0.06	0.11
MnO	0.28	0.21	0.23	0.23	0.25	0.21	0.22	0.23	0.26	0.23	0.23	0.26	0.16	0.24	0.24	0.26	0.29	0.31	0.29	0.19	0.16	0.16	0.20	0.23	0.27	0.22
Total	100	100	100	100	100	100	100	100	100	100	100	100	100	100	100	100	100	100	100	100	100	100	100	100	100	100
LOI	10.4	3.59	3.61	3.2	3.84	2.87	3.04	3.3	1.92	2.3	2.86	9.21	3.58	2.74	2.34	2.16	2.52	2.74	9.7	3.36	2.87	4.06	3.97	1.6	3.08	3
Fe#	1.12	1.40	0.64	1.10	0.73	1.08	0.93	0.97	0.95	0.76	0.75	1.52	2.29	4.07	2.47	2.31	2.15	1.96	3.81	1.31	2.07	7.28	3.50	3.76	2.34	2.67

	27	28	29	30	31	32	33	34	35	36	37	38	39	40	41	42	43	44	45	46	47	48	49	50	51	52
Sample	C-33	B-938	B-939	B-959	B-960	B-961	C-19a	C-15	C-16a	C-16 6	3059	C-26 B	2555	2579a	83-9/9	83-6/4	83-6/2	83-6/3	83-9/8	$920/7_3$	$920/12_3$	C-1	T-1	M-2	M-1	B-1
SiO_2	56.26	48.24	52.96	55.71	51.51	53.63	57.84	54.43	55.08	55.74	56.77	55.40	55.14	62.39	54.90	55.41	56.21	56.33	59.50	57.76	61.51	57.80	54.83	56.93	58.48	58.67
Al_2O_3	17.62	8.26	16.47	18.33	18.31	17.79	12.92	13.50	14.42	14.13	9.34	14.81	16.32	10.09	13.25	12.95	12.99	13.44	12.28	14.89	10.71	11.93	11.14	16.04	11.30	11.07
TiO_2	0.87	0.17	0.37	0.84	1.45	0.69	0.33	0.29	0.42	0.39	0.24	0.44	0.33	0.24	0.17	0.16	0.21	0.23	0.14	0.23	0.16	0.21	0.35	0.33	0.22	0.14
P_2O_5	0.10	0.02	0.03	0.08	0.30	0.08	0.06	0.03	0.04	0.04	0.03	0.15	0.05	0.05	0.04	0.04	0.04	0.09	0.04	0.00	0.00	0.04	0.12	0.07	0.03	0.02
FeO*	11.98	19.41	9.23	13.81	10.67	10.32	8.56	8.89	8.56	8.98	8.72	7.91	7.25	5.77	8.83	8.36	8.91	8.44	7.88	7.85	6.90	8.74	8.49	7.25	8.58	8.46
CaO	3.50	11.51	8.65	1.28	6.55	6.74	6.05	8.26	6.65	9.83	6.15	9.58	5.11	6.43	5.79	6.42	7.83	4.68	5.69	7.17	7.17	7.04	8.46	5.46	6.30	7.77
MgO	3.89	10.93	7.89	3.51	8.60	5.47	9.04	12.22	10.70	9.25	16.83	8.86	12.10	10.48	14.00	14.68	12.11	13.34	11.26	8.08	10.46	11.22	14.99	10.75	12.34	11.69
Na_2O	5.45	0.83	3.82	6.09	1.90	4.36	4.95	1.90	3.77	1.41	1.66	2.59	3.23	4.16	2.82	1.81	1.54	3.15	2.96	3.49	2.80	2.03	1.16	2.25	1.85	1.61
K_2O	0.04	0.34	0.41	0.26	0.55	0.77	0.05	0.29	0.24	0.08	0.06	0.11	0.26	0.27	0.05	0.02	0.02	0.14	0.12	0.40	0.18	0.85	0.27	0.81	0.71	0.42
MnO	0.29	0.30	0.17	0.07	0.16	0.16	0.20	0.17	0.13	0.17	0.19	0.15	0.20	0.11	0.16	0.16	0.15	0.14	0.14	0.12	0.11	0.15	0.18	0.12	0.19	0.17
Total	100	100	100	100	100	100	100	100	100	100	100	100	100	100	100	100	100	100	100	100	100	100	100	100	100	100
LOI	5.65	4.4	3.49	4.59	7.67	8.66	1.96	3.08	3.44	2.76	5.38	3.01	3.79	7.1	4.62	4.92	4.39	4.34	3.92	2.23	3.29	3.81				1.03
Fe#	3.08	1.78	1.17	3.94	1.24	1.89	0.95	0.73	0.80	0.97	0.52	0.89	0.60	0.55	0.63	0.57	0.74	0.63	0.70	0.97	0.66	0.78	0.57	0.67	0.69	0.72

Note: 1-12 – Uimen-Lebed boninites, 13-32 – Uimen-Lebed basaltic volcanics/andesites (13-27) and gabbro (28-32) (Buslov et al., 1997), 33-36 – boninites of West Sayan (Buslov et al., 1993), 37-40 – boninites of East Sayan (Belichenko et al., 1988), 41-47 – Khan-Taishirin boninite (Mongolia) (Kepezhinskas et al., 1987), 48-52 – average boninite compositions: C-1 – from (Bogatikov, 1987), T-1 – Tonga arc (Vysotsky, 1989), M-1 – Mariana arc, M-2 – Mariana trench, B-1 – Bonin Island (Bogatikov, 1987; Vysotsky, 1989).

have a thick sedimentary cover (black shale and carbonate turbidites) with a large amount of clastic material. On the contrary, oceanic ophiolites are poorly preserved and exposed, and their fragments are frequently mélanged and incorporated into accretionary wedges.

Boninite series rocks compose variable volcanic and subvolcanic bodies. However, the majority of boninite localities are in sheeted dyke units ("dyke-in-dyke" complexes). Boninites were formed at the last stage of the development of sheeted dyke units.

Our studies of the Gorny Altai ophiolites showed that tectonic events with the participation of boninite magma started with the spreading, which is recorded by the formation of "dyke-in-dyke" units, and lead to the formation of volcanic complexes intruded by variably-oriented dykes and sills. Moreover, boninites serve as a connecting link between spreading and volcanism: they are the last to form in the zones of spreading and the first in dyke-sill complexes, where boninites are preserved as screens.

Geochemical investigation of major and trace element concentrations showed that volcanics in association with boninite series in the Kurai Range have characteristics of island arc tholeiites and calc-alkaline series (Simonov et al., 1994; Buslov et al., 1998). The REE patterns are depleted in LREE with respect to MREE and HREE.

Vendian-Cambrian boninites are clearly depleted in REE, and mostly in LREE, compared to tholeiites and calc-alkaline volcanics. This possibly indicates the more primitive character of old boninite magmas in the active margin of the Paleo-Asian ocean compared to the present boninite melts in the Pacific ocean (Simonov et al., 1994).

Thus, REE and major element geochemistry of Vendian-Cambrian rocks of the Kurai Range indicate several volcanic series from more evolved MORB through boninites and island arc tholeiites to calc-alkaline series. This reflects a successive evolution of the primitive island arc and then more evolved island arc formed over the oceanic crust of the Paleo-Asian ocean.

Three Stages of Island Arc Evolution

Judging from the biostratigraphical and sedimentological data documented in the Anui-Chuya fore-arc trough, it is obvious that in the Middle–late Cambrian, the pre-existed island arc crust and accretionary wedges had been subjected to erosion. One of the Ar–Ar dating results show the episode of Vendian exhumation of eclogite. It may be concluded that the metamorphic boulders found in the Anui-Chuya trough are of pre-Vendian rocks.

Three stages of the evolution of the Siberian continent island arc margin may be discriminated. During *the Vendian subduction stage (1)* an ensimatic active margin formed close to the Siberian continent. In Vendian time, the subduction of the oceanic crust of the Paleo-Asian ocean resulted in the formation of the Uimen-Lebed primitive island arc. Oceanic islands and seamounts migrated towards the subduction zone and collided with the island arc. It caused the closure of the subduction zone and initiation of reverse flows in the accretionary wedge. Metaperidotites of the Chagan-Uzun massif and eclogite-bearing serpentinitic mélange were exhumed along the slope of the island arc. The oceanic islands and seamounts were incorporated in the accretionary wedge and the subduction zone jumped oceanwards.

The Cambrian arc (2) resulted in the formation of a more evolved island arc composed of calc-alkaline volcanics and granites. A fore-arc trough formed in Middle–late Cambrian time and was filled with disrupted products of Vendian-Middle Cambrian accretionary wedges and island arcs.

The *Tremadoc collision (3)* of the more evolved island arc with the Siberian continent is documented by Tremadoc folding, metamorphism and intrusion of granites (Vladimirov et al., 1997). The time span between primitive island arc and mature arc which is demonstrated by activity of calc-alkaline rocks are only a few millions of years in the case of Izu-Bonin island (Taylor, 1992) and the stage (1) and (2) may be partly overlapped.

In the late Paleozoic, the Caledonian accretion-collision structure of the Siberian continent was broken by large-scale strike-slip faults into several segments. This resulted in the formation of a typical mosaic-blocky structure.

The whole set of paleo-oceanic island units, olistostromes, ophiolites and high-pressure units that has been found in the Kurai zone, allows a reconstruction of paleogeodynamic processes in the early stages of the formation of ASA folded zones. The mode of evolution was similar to that of the western Pacific active margin (Buslov et al., 1993; Watanabe et al., 1993; Buslov and Watanabe, 1996).

Summary

The early Caledonian accretion-collision zones of Gorny Altai are composed of the rock units, which formed within an island arc system or were incorporated in it during the subduction of the Paleo-Asian ocean crust under the Siberian continent. They are accretionary wedge, fore-arc trough, primitive and more evolved island arc and back-arc basin units. The accretionary wedges are characterized by a sheeted structure and consist of ophiolites from the basement of an island arc and the rocks of a deformed oceanic crust (the Paleo-Asian oceanic plate). We propose a general scenario implying that oceanic islands submerged into the subduction zone

together with the plate and, later, they were incorporated into an accretionary wedge. During the subduction, the oceanic islands – the largest ones were upto 4 km in height – collided with an island arc resulting in the reverse currents in the accretionary wedge and their related exhumation of high-pressure rocks (blueschists, eclogites, etc.). In response to the paleoseamount/island arc collision, the subduction zone jumped oceanwards. The fragments of paleoseamounts in the accretionary wedge are as a rule, cemented by olistostromes consisting of broken seamount and island arc units. A new volcanic arc formed over the accretionary wedge. Fore-arc basins were filled with pelagic sediments and turbidites up to 6–8 km thick. The turbidites are mainly composed of the fragments and debris of island arc and accretionary units.

Temporal and lateral polarity of magmatic rocks is typical of volcanic arcs: tholeiite-boninite series of the early stage (Vendian-the earliest early Cambrian), which are similar to the Bonin islands, Mariana arc, and Tonga arc, and tholeiite-calc-alkaline and, to a lesser degree, calc-alkaline arc volcanic series of the later stage. Laterally, various volcanic units are recognized within large fragments of more evolved island arcs ranging in composition from tholeiitic (high-Mg andesite and basalt) in frontal parts, through calc-alkaline in central parts to shoshonitic in back-arc areas (Buslov et al., 1993; Simonov et al., 1994).

Thus, Vendian-Cambrian units in the Gorny Altai are those of (1) Vendian seamounts formed over within-plate hot spots of the Paleo-Asian ocean including N-MORB and E-MORB lavas, (2) the fragments of the Vendian primitive boninite-tholeiitic island arc and (3) the Cambrian more evolved island arc with a fore-arc basin.

There, we can reconstruct the collisional processes occurring in a subduction zone due to the collision of large seamounts with an island arc. The evolution of early Caledonian accretion-collisional processes can be exemplified by the Kurai zone in Gorny Altai. The fragments of a Vendian island arc, Vendian–early Cambrian accretionary wedge and Cambrian fore-arc basin have been preserved in this territory. Cambrian more evolved island arc units are found only as rare intrusive bodies and dykes. The Cambrian more evolved island arc units (Buslov et al., 1993) are well exposed northward, in Central Gorny Altai, Salair, and Kuznetsk Alatau (Buslov et al., 2001).

The correlation of structural, lithological, geochemical and biostratirgaphic data shows that an extended island arc system of the present western Pacific type existed at the margin of the southwestern Siberian continent in Vendian-Cambrian time. Further detailed lithological, paleomagnetic and geochemical investigations would permit the learning of the specific features of the geodynamic evolution of the Paleo-Asian ocean and the reconstruction of its boundaries and paleogeographic position.

Acknowledgment

We would like to express our thanks to Prof. N.L. Dobretsov for his leadership in organizing Russian-Japan co-operative work since 1992. Our thanks are extended to Prof. Y. Hariya for his understanding of the significance of our scientific exchange program. Without their support our joint research could not have been be carried out.

Prof. T. Itaya, Okayama University of Science, has continuously encouraged our dating program (K–Ar dating study) and we have got significant information from his laboratory. The discussions with Dr. Ota were also very useful.

Prof. S. Maruyama supported a part of the field expenses. We acknowledge the support and encouragement of the staff in UIGGM and Division of Earth and Planetary Sciences, Hokkaido University as well as of all the scientists mentioned above. We also benefited from comments by Dr. S.A. Pisarevsky and Dr. Victor Kovach.

The work was supported by the Russian Foundation for Basic Research, Grants Nos. 01-05-65090 and 02-05-64627.

References

Akiyama, M. (1994) The isotope ages and P–T paths of high-pressure rocks in serpentinite mélange from Chagan-Uzun, Altai mountain and the Chara ophiolite belt, Kazakhistan. Hor. thesis, Hokkaido University (unpublished thesis, in Japanese with English abstract). 100p.

Belichenko, V.G., Butov, Yu.P. and Boos R.G. et al. (1988) Geology and metamorphism of East Sayan. Novosibirsk, (in Russian).

Berzin, N.A. and Dobretsov, N.L. (1994) Geodynamic evolution of southern Siberia in late Precambrian–early Paleozoic time, in reconstruction of the Paleo-Asian ocean. In: Coleman, R.G. (Ed.), Utrecht, The Netherlands, pp. 53-70.

Bogatikov, O.A. (1987) Petrology and geochemistry of island arcs. Nauka, Moscow, (in Russian).

Bondarenko, P.M. (1976) Modeling of thrust faulting in folded areas. Novosibirsk, 109p (in Russian).

Buslov, M.M. (1992) Tectonic nappes of Gorny Altai. Novosibirsk, 95p (in Russian).

Buslov, M.M. and Sintubin, M. (1995) Structural evolution of the Lake Teletskoe zone, Altay-Sayan folded area. Russian Geol. Geophys., v. 36, pp. 81-87.

Buslov, M.M. and Watanabe, T. (1996) Intrasubduction collision and its role in the evolution of an accretionary wedge: the Kurai zone of Gorny Altai, Central Asia. Russian Geo. Geophys., v. 36, pp. 83-94.

Buslov, M.M., Saphonova, I.Yu. and Bobrov, V.A. (1997) New geochemical data on boninites from Kurai ophiolites, Gorny Altai. Dokl. Ros. Acad. Nauk, v. 361, pp. 244-247.

Buslov, M.M., Berzin, N.A., Dobretsov, N.L. and Simonov, V.A. (1993) Geology and tectonics of Gorny Altai. Novosibirsk, UIGGM Publ., Novosibirsk, 122p.

Buslov, M.M., Sennikov, N.V., Iwata, K., Zybin, V.A., Obut, O.T., Gusev, N.I. and Shokalsky, S.P. (1998) New data on the structure and age of olistostromal and sand-silty rock masses of the Gorny Altai series in the southeast of the Gorny Altai, Ahui-Chuya zone. Russian Geol. Geophys., v. 39, pp. 801-809.

Buslov, M.M., Saphonova., I.Yu., Watanabe, T., Obut, O.T., Fujiwara, Y., Iwata, K., Semakov, N.N., Sugai, Y., Smirnova, L.V., Kazansky, A.Yu. and Itaya, T. (2001) Evolution of the Paleo-Asian ocean (Altai-Sayan region, Central Asia) and collision of possible Gondwana-derived terranes with the southern marginal part of the Siberian continent. J. Geosci., v. 5, No. 3, pp. 203-224.

Didenko, A.N. (1997) Paleomagnetism and geodynamic evolution of the Ural-Mongolian foldbelt. Dr. Sci. Thesis, United Institute of Earth's Physics, Moscow, pp. 1-52.

Didenko, A.N., Mossakovsky, A.A., Pechersky, D.M., Ruzhenstev, S.V., Samygin, S.G. and Kheraskova, T.N. (1994) Geodynamics of the Central Asia Paleozoic oceans. Russian Geol. Geophys., v. 35, pp. 59-75.

Dobretsov, N.L., Berzin, N.A. and Buslov, M.M. (1995) Opening and tectonic evolution of the Paleo-Asian ocean. Int. Geol. Rev., v. 35, pp. 335-360.

Fedorov, A.B. and Pereladov, V.S. (1987) Siliceous sponge spicules from the Kuonam Formation of the north-eastern Siberian Platform. In: New species of the fossils of Phanerozoic plants and invertebrates in Siberia, SNIIGGIMS Publ., Novosibirsk, pp. 36-46 (in Russian).

Gusev, N.I. (1985) Volcanic rocks in eastern Gorny Altai. Geol Geophys., No. 5, pp. 28-35 (in Russian with English abstract).

Gusev, N.I. (1987) Petrochemistry of the Arydzhan suite in southeastern Gorny Altai. In: Magmatism and endogenic metallogeny of western Altai-Sayan folded area, Novokuznetsk, pp. 75-77 (in Russian).

Gusev, N.I. (1991) Reconstruction of geodynamic regimes for Precambrian and Cambrian volcanism in southeastern Gorny Altai. In: Kuznetsov, P.P. et al. (Eds.), Paleogeodynamics and formation of mineral-rich zones in South Siberia, pp. 32-54 (in Russian).

Gusev, N.I. and Khalitova, Z.A. (1988) Model detritus composition of sandstones of the Gornoaltaiskaya Series in the south-eastern part of the Anui-Chuya syncline and the character of provenance. In: Mineral resources in Altai: new prospects and development, Barnaul, pp. 14-16.

Gusev, N.I. and Kiselev, E.A. (1988) A Precambrian stratigraphic sequence in southeastern Gorny Altai. In: Late Precambrian and early Paleozoic deposits in Siberia, Riphean and Vendian, Inst. Geol. and Geophys., Novosibirsk, pp. 125-134 (in Russian).

Kepezhinskas, K.B., Kepezhinskas, V.V. and Zaistev, N.S. (1987) Precambrian–Cambrian evolution of the earth crust of Mongolia. Nauka, Moscow (in Russian).

Kuznetsov, P.P. (1980) Structural features of ultramafic belts in Altai-Sayan area, Novosibirsk, 95p.

McKerrow, W.S., Scotese, C.R. and Brosier, M.D. (1992) Early Cambrian continental reconstructions. J. Geol. Soc. London, v. 149, pp. 589-606.

Meschede, M. (1986) A method of discriminating between different types of mid-ocean ridge basalts and continental tholeiites with the Nb-Zr-Y diagram. Chem. Geol., v. 56, pp. 207-218.

Nicolas, A. (1989) Structure of ophiolites and dynamics of oceanic lithosphere. Kluwer Ed., 367p.

Ota, T., Buslov, M.M., Maruyama, S., Utsunomiya, A. and Ishikawa, A. (2000) Precambrian high-P/T metamorphism in the Gorny Altai, southern Russia, and its tectonic implication. Eos Trans. AGU, v. 81, Fall Meet. Suppl., Abstract V21E-19.

Perfiliev, E.E., Gusev, N.I. and Gutak, Ya.M. (1994) Age of the olistostrome in the Anuy-Chuya depression (Gorny Altai). In: Geodynamics of southern Siberia, Tomsk, p. 58 (in Russian).

Petrunina, Z.E., Sennikov, N.V. and Ermikov, V.D. et al. (1984) Lower Ordovician stratigraphy of Gorny Altai. In: Lower Ordovician stratigraphy and fauna of Gorny Altai, Moscow, p. 3 (in Russian).

Rollinson, H.R. (1993) Using geochemical data: evaluation, presentation, Interpretation. Longman Group UK Ltd., 352p.

Scotese, C.R. and McKerrow, W.S. (1990) Revised world maps and introduction. Geo. Soc. Mem. No. 12, pp. 1-21.

Sengor, A.M.C., Natal'in, B.A. and Burtman, V.S. (1993) Evolution of the Altaid tectonic collage and Paleozoic crustal growth in Eurasia. Nature, v. 364, pp. 299-307.

Simonov, V.A., Dobretsov, N.L. and Buslov, M.M. (1994) Boninite series in structures of the Paleo-Asian ocean. Russian Geol. Geophys., v. 35, pp. 182-199.

Taylor, B. (1992) Rifting and the volcanic-tectonic evolution of the Izu-Bonin-Marina arc. In: Taylor et al. (Eds.), Proceedings ocean drilling program, scientific results, v. 126, pp. 627-651.

Uchio, Yu., Isozaki, Yu., Nohda, S., Kawahata, H., Ota, T., Buslov, M.M. and Maruyama, S. (2001) The Vendian to Cambrian Paleo-environment in shallow mid-ocean: stratigraphy of Vendo-Cambrian seamount-top limestone in the Gorny Altai mountains, southern Russia. Gondwana Res., v. 4, pp. 47-48.

Vladimirov, A.G., Shokalsky, S.P. and Ponomareva, A.P. (1996) Riftogenic and strike-slip nature of late Paleozoic–early Mesozoic granites in Altai. Dokl. RAN, v. 350, pp. 83-86 (in Russian).

Vladimirov, A.G., Ponomareva, A.P., Shokalsky, S.P., Khalilov, V.A., Kostitsyn, Yu.A., Ponomarchuk, V.A., Rudnev, S.N., Vystavnoy, S.A., Kryk, N.N. and Titov, A.V. (1997) Late Paleozoic–early Mesozoic granitoid magmatism in Altai. Russian Geol. Geophys., v. 38, pp. 715- 729.

Volkov, V.V. (1966) Main features of the geological evolution of Gorny Altai. Novosibirsk, 162p (in Russian).

Vysotsky, S.V. (1989) Ophiolitic associations of Pacific island-arc systems. Vladivostok (in Russian).

Watanabe, T., Buslov, M.M. and Koitabashi, S. (1993) Comparison of arc-trench systems in the early Paleozoic Gorny Altai and the Mesozoic–Cenozoic of Japan. In: Coleman, R.G. (Ed.), Reconstruction of the Paleo-Asian ocean, VSP Intern. Sci. Publ., The Netherlands, pp. 160-177.

Zonenshain, L.P., Kuzmin, M.I. and Natapov, L.M. (1990) Geology of the USSR: a plate tectonic synthesis. Geodynamic Monograph, American Geophysical Union, Washington, 242p.

Zybin, V.A. (1985) Lower Paleozoic olistostromes of the central part of Gorny Altai. In: Geology and mineral deposits of the Altai territory. Biysk, pp. 12-15 (in Russian).